universität wien

MASTERARBEIT / MASTER'S THESIS

Titel der Masterarbeit / Title of the Master's Thesis

Towards Understanding A Sandpile Model As A Sample Space Reducing Process

verfasst von / submitted by

Simon Rella, BSc

angestrebter akademischer Grad / in partial fulfilment of the requirements for the degree of

Master of Science (MSc)

Wien, 2021 / Vienna, 2021

Studienkennzahl lt. Studienblatt / degree programme code as it appears on the student record sheet:	UA 066 876
Studienrichtung lt. Studienblatt / degree programme as it appears on the student record sheet:	Masterstudium Physik
Betreut von / Supervisor:	Univ.-Prof. Mag. Dr. Dr. Stefan Thurner

Acknowledgements

I want to thank Univ.-Prof. Stefan Thurner for supervising my research and guiding the writing process. During my thesis work I was closely supervised by Dr. Rudolf Hanel and I wish to thank him for the countless discussion we had, his emotional support and for holding the torch. Univ. Prof. Christoph Dellago from the University of Vienna was so kind and co-supervised this thesis.

I am in debt to all the friends and colleagues from the Complexity Science Hub Vienna that supported me during the time of my thesis work.

Lastly, I will express my thanks to Anna Berezhinskaya.

Contents

1 Thermodynamics Out Of Equilibrium

What are the thermodynamic conditions for life to sustain itself? What can we learn about the atmosphere of our planet as a dynamically evolving system? How will the stock market look like the day after tomorrow? How did a galactic gaseous nebula structure itself? Are there general methods or laws that allow us to classify and predict dynamical systems?
The challenges of nonequilibrium systems have stimulated a broad spectrum of experimental and theoretical work. For a thermodynamic system near a local equilibrium that is driven by small forces Ilya Prigogine [1], based on works of Lars Onsager [2], predicted a balance of fluxes, which he identifies as the steady state of the system, given that the entropy production $\dot{S}$ is minimal,

$$J_{m,in} = J_{m,out} \qquad \frac{\partial \dot{S}}{\partial X_m} = 0 \qquad . \tag{1.1}$$

E. T. Jaynes commented on Prigogine's computations in 1980 [3]. He criticized that *the final Euler-Lagrange equations expressing minimum entropy production reduce simply to the conservation laws.* In fact Eq. (1.1) can be seen as a statement about the conservation of fluxes.
Central to Prigogine's theory is the use of fluxes as major entities in such driven systems. But the fluxes he defined are small. In this thesis we will be exploring a system that gives rise to large fluxes. In order to account for those, an extended tool set will be required.

Jaynes

Nevertheless Prigogine's theory proofed to be useful in certain applications, in which the strong assumption of small perturbations around a local equilibrium, is valid. In other cases, different extremal principles may give better results (see review [4]). In the end however, none of these theories were able to proof themselves as universally applicable.
Jaynes proposed to use concepts of information theory and statistical inference [5] in order to advance. Out of all possible trajectories a dynamical system could undergo, we shall find the one which is most probable given the information we have. Adopting the Bayesian standpoint, Jaynes sees probabilities just as an expression of our expectation about an outcome. At first sight there may be many different probability distributions that match our finite set of expectations (constraints) about the system. The mathematical task at hand however is one in which we wish to find the probability distribution of paths x_i that leaves us in a state of least knowledge about which path was actually chosen given our constraints. The thought for distribution only contains information we have about the system. A measure for the information content of a probability distribution was found by Shannon and also called "entropy" $-S_I$ due to its

close resemblance of thermodynamic entropy,

$$S_I = -\sum_i^W p(x_i) \log p(x_i) \qquad . \tag{1.2}$$

Jaynes called this approach "maximum caliber" in contrast to the similar "maximum configuration" approach in the case of scalar entities x_i. [6] and [7] recently showed that Prigogine's theorem, Eq. (1.1), can be derived from a maximum caliber approach. The authors note that maximum caliber *does not require any notion of local equilibrium, or any notion of entropy dissipation, or temperature, or even any restriction to material physics, it is more general than many traditional approaches.*

The thermodynamics of self-organized systems

It is promising to study self-organized dissipative systems in such a framework of paths or calibers. Like in classical statistical mechanics, which is mainly concerned with equilibrium thermodynamics that links microscopic quantities with a macroscopic description one could also hope to describe dissipative systems statistically by connecting microstates with macro variables, which in the case of a self-organizing system will typically be more complicated than states of an isolated equilibrium system. In particular the dynamics of microstates in such self-organising systems can be expected to violate basic principles of equilibrium thermodynamics like ergodicity or detailed balance.
Prigogine's analysis was limited to a single attractive point in phase space, that is defined by the equality of inflow and outflow, Eq. (1.1). A real dissipative system however is able to reallocate and store energy, transform the accessible phase space and allow for dynamic behaviour of the macro variables. At a sufficiently fine resolution systems driven by a flux through may reveal "stochastic limit cycles", that are even more complex stochastic attractors. The "steady state" then is nothing but a long time average of system observables.
In the following thesis I will present some of the mentioned aspects of non-equilibrium phenomenology with the concrete example of sandpile dynamics and in particular the Oslo sandpile model. These systems, as proponents of a larger class of self-organized systems, will be extensively examined in this thesis.

Sandpile models

A well studied example for a non-equilibrium system with a steady state are piles of granular matter. See figure 1 for a visual representation. If I continuously drop grains at a given position, a cone of sand will form. After a while the basis angle of the cone will reach a limiting value. If the slope is too steep, avalanches will emerge. If it is too shallow, the pile will build up further. In the steady state the inflow of sand on average equals the outflow. The fluctuation size of certain macro variables shows power law distributions, which attracted considerable interest within the scientific community ([8], [9]). These distributions pose a

need for novel thermodynamic descriptions that can account for non-Gaussian statistics and the present work will explore one possible approach.
The traditional way to treat this situation physically is by invoking the concept of self-organized criticality [8]. In this thesis however I investigate an alternative route to non-equilibrium dynamics using concepts of Sample Space Reducing Processes (SSR) [1]. Those focus on constraints in dissipative systems, that limit the structure and dynamics of sampling spaces underlying those systems. To summarize, it is the main aim of my work to measure and derive SSR-characteristics of the Oslo model.

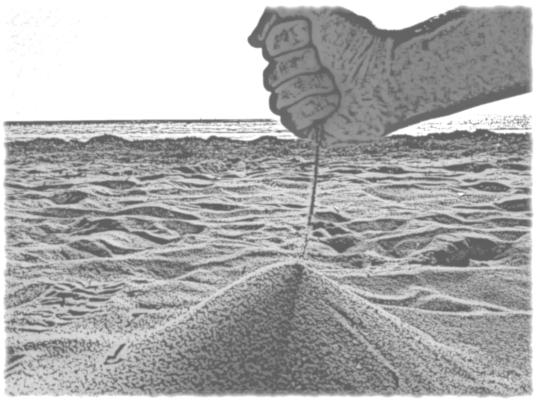

Figure 1: A sandpile building up by continuous inflow of sand. Picture taken on a beach near Grado (Italy).

Content of the present work

The present thesis will be structured as follows: In the second and third section I will give an introduction to a particular numeric model for sandpiles, namely the Oslo sandpile model. We will review the classical treatment using the concept of self-organized criticality and study its basic structure on a macroscopic and microscopic level. This will illustrate the non-equilibrium nature of sandpiles.
The fourth section will present sample space reducing processes in a formal way. I will discuss different forms of such processes. The connection of this approach to Jaynes' "maximum entropy configuration" will be addressed. Finally by the end of that section I will construct a connection between SSR processes and sandpiles by identifying the abstract notion of state in the SSR framework with concrete variables taken from the Oslo model.
In the fourth section I summarize the main results of my analysis of sandpile dynamics, in which I describe in detail how the Oslo model in particular can be understood through SSR processes.

2 Sandpiles As Self-organized Critical Systems

This thesis is dealing with a physical model for the surface of a pile of granular matter. P. Bak, C. Tang and K. Wiesenfeld (BTW) proposed a simple computational toy model (BTW model) for the dynamics of such a pile of sand in 1987 [8]. The model consists of a rectangular table onto which grains of sand are dropped at random positions. The table features a Cartesian grid, such that each position x_{ij} in the grid has the size of a grain. Over time the grains would start to tower up. By reaching a certain threshold in height the tower collapses and the grains are transported from grid position x_{ij} to its nearest neighbours $\{x_{i+1,j}, x_{i-1,j}, x_{i,j+1}, x_{i,j-1}\}$. There it may trigger another collapse or a whole chain of collapses. Once the system has reached a stable configuration again, a new grain is dropped onto the table. If a grain reaches the boundaries of the table, it falls off the edge and disappears.
Over time the system reaches a dynamic equilibrium where the amount of grains entering the system, averaged over long times, equals the amount of grains departing the system. The total mass M is on average conserved,

$$\langle \Delta M_{in} \rangle \approx \langle \Delta M_{out} \rangle \qquad . \tag{2.1}$$

While this is the sort of dynamical equilibrium that Prigogine's theorem recovers from the minimization of "Entropy Production", the theorem does in fact not apply to the dynamics emerging from this model. The fluctuations of most quantities in the model span many orders of magnitude and it would be incorrect to project them into a linear regime governed by detailed balance. This we will in further depth see by the end of section 3.
The fluctuations are in fact the quantity most studied in the BTW model, particularly the length of chain reactions occurring. Here the avalanche size s is defined as the amount of consecutive unstable states until the system reaches a stable configuration. If we call $X(t)$ the stable configuration at time t and $X^\star(t+1)$ an unstable configuration at time $t+1$ (reached via a grain dropping onto the pile) then we can write schematically for one relaxation event

$$X(t) \to X^\star(t+1) \to X^\star(t+2) \to \cdots \to X^\star(t+s-1) \to X(t+s) \qquad .$$

BTW [8] found that the probability $p(s)$ has the statistics of a power law with roughly an exponent $\alpha = -1$ in their model. $\alpha = -1$ actually was later shown to be the incorrect value by Christensen et. al. [10] - and rather an exponent $\alpha = -2$ should apply. The general claim, of the power spectrum to have a power law distribution, Eq. (2.2), remains,

$$p(s) \propto \frac{1}{s^\alpha} \qquad . \tag{2.2}$$

This so called $1/f$-noise, sometimes also referred to as pink noise, appears to be very widespread in nature. BTW name transport times in the hour glass, flows of the river Nile & the luminosity of stars [11]. If s is not measured in time,

but in space, also fractal spatial patterns will obey such power law statistics in the distribution of structure sizes (eg. river basins, snow flakes, broccoli, etc.). One could add many more examples from almost all scientific disciplines. It however remains a taunting question whether or not have we identified all mechanisms that can trigger the emergence of $1/f$-noise. BTW introduced, supported by their computational results, the concept of self-organized criticality (SOC). To which extend other $1/f$-noise producing mechanisms such as preferential attachment [12], multiplicative processes [13] and recently SSR processes are equivalent/different to this traditional approach is still a matter of research. In section 4 I will explore the theory of SSR processes. SOC, as the traditional approach, shall be briefly revisited now.

2.1 Self-organized criticality

While most standard equilibrium statistical physics problems are related to distributions with finite second moment (such as the exponential Gibbs-Measure, Gaussians, Maxwellians, ...), systems with a correlated Hamiltonian, can also provide power law distributions. They can often be observed for thermodynamics near a phase transition. A prominent example is the Ising model for the magnetic properties of a metal [14]. Below a certain temperature T_c the metal appears non-magnetic, above it is. The transition occurs as the result of interacting little magnets of atomic scale. At low temperatures (low noise) the atomic magnets form one large block with all magnets pointing in the same direction (magnetic), while at high temperatures long range correlations vanish and the chaotic orientations do not create an overall magnetic field. Systems with T_c however form correlated domains of all sizes. The system becomes self-similar and the distribution of correlation-lengths (the sizes of domains with the same orientation) becomes a power law [15].
While in equilibrium statistical physics, one has to fine-tune the system temperature to become $T = T_c$, the idea of SOC is that some non-equilibrium systems might be inherently attracted towards criticality.
The ideas of SOC found plenty of applications [16], but also raised considerable controversy [17]. While the inventors speculated about SOC to be a universal mechanism to create fractal patterns [18], the core claim ("self-tuned phase transitions can (and do) exist in nature" [17]) was even extended by some proponents to explanations of power laws and dissipative systems in general. There are on the other hand many alternative routes explaining the emergence of power laws of various kinds, including multiplicative processes (as in [13]), preferential mechanisms (as in [12]) or sample space reducing processes (which will be discussed in the next chapter). To which extent these other $1/f$-noise producing mechanisms can be unified or used as alternative descriptions of the same phenomena is still under investigation.

In a critical review, conducted 25 years after BTW's observations were made, the authors write [17]:

> *Unless one accepts the claim that SOC is the basis of scaling in nature, SOC itself (not just scaling) [...] is difficult to identify in a natural phenomenon or experiment directly. If anything, SOC has been offered as an explanation for certain scaling to appear spontaneously. At the theoretical end, none of even the computer models which are widely accepted as displaying all the hallmarks of SOC has been solved or even only systematically approximated. [...]. To this day, there is no complete theory of SOC and it remains unclear why a phenomenon, that should be observable under generic conditions is so rarely seen.*

A particularly well studied SOC computer model is the Oslo sandpile model, which will be discussed in the following.

2.2 Experimental evidence

The Oslo sandpile model (OSM) was motivated by rice pile experiments, which were first conducted in Oslo [9]. Rice was chosen in the experiment as granular matter. Real spherical sand turned out not to be viscose enough to reproduce critical distributions. The experimental setup is sketched in figure 2.

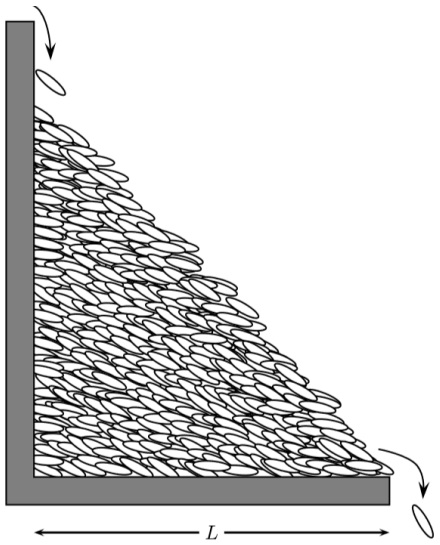

Figure 2: Illustration of the experiment in Oslo. Rice enters the system on one the peak of the pile and can leave the system at the other end of the table.

The 1+1 Dimensional system receives a grain of rice with average size l dropped onto it on one end of a table with length L. After a while grains of rice can leave

the system by toppling from the table on the other end. The system will evolve into a semi-steady state characterized by a flow balance of incoming and outgoing grains: The critical state. The sizes of avalanches s are measured as the amount of internally toppled grains of rice, which dissipate an average energy of $\Delta E \approx mgl$. Power law distributions of s are found in the experiment. The correlations of different sites in the pile diverge as the pile reaches the steady state. Instabilities in the origin of the pile can be carried towards the end within one relaxation event. Figure 3 shows the resulting distribution of s as presented in [19]. A power of $\tau \approx -2$ is found.
The experimental findings then inspired numeric simulations, that I will discuss next.

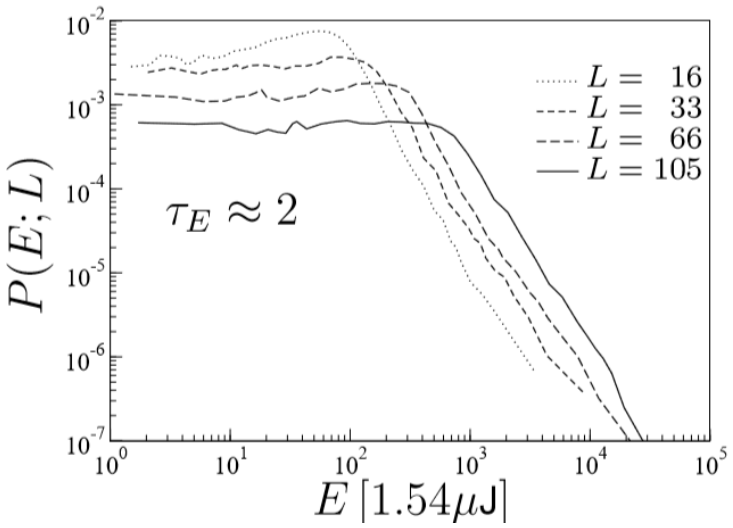

Figure 3: The typical power law found in the experiments conducted in Oslo. The horizontal axis shows the size s of an avalanche, the vertical axis is proportional to the frequency. τ, here the exponent of the power law fit, is found to be around -2. [Complexity and Criticality, Christensen and Moloney, Copyright @ 2005 Imperial College Press]

2.3 Description of the Oslo sandpile model

The OSM is a simplified discrete model for the dynamics based on the steepness (slope) k of a certain position x in 1D. During each driving process the steepness of $x = 1$ (leftmost site) is increased by one:

$$k(1) \rightarrow k(1) + 1 \qquad .$$

A random number $\eta(x)$, either one or two, is chosen for all sites with probability

p or $(1-p) = q$. If a local slope at x is larger than the random number $\eta(x)$, an avalanche occurs. The random process $\eta(x)$ therefore characterizes the local stability of the pile. During an avalanche event the slope of $x+1$ and $x-1$ is increased by one, while the slope of x is reduced by two:

$$\begin{aligned} k(x) &\to k(x) - 2 \quad , \\ k(x+1) &\to k(x+1) + 1 \quad , \\ k(x-1) &\to k(x-1) + 1 \quad . \end{aligned}$$

One says, site x has toppled. The toppled site also updates its local stability to 1 or 2 with probability p:

$$\eta(x) \to \begin{cases} 1 & \text{with prob. } p \\ 2 & \text{with prob. } 1-p \end{cases} \quad .$$

At a boundary $x = L$ the grains fall off the table. Therefore we have

$$\begin{aligned} k(L) &\to k(L) - 1 \quad , \\ k(L-1) &\to k(L-1) + 1 \quad . \end{aligned}$$

Afterwards, new stability values are assigned to those states that just engaged in toppling. The process continues until all local stability criteria are met. At this point the process has to be driven again by dropping a grain for more relaxation steps to follow. The dynamics are visualized and summarized in figure 4.
This is equivalent to other formulations using the height $H(x)$ or the active height $h(x)$ of a site. $h(x)$ is the height above the absolutely stable height: $h(x) = 0$ translates to a real height of $H(x) = x$. It holds that $k(x) = h(x) - h(x+1)$.

Details about the algorithm

Regarding the computational realization one can make use of the Abelian property of the relaxation process. Having the Abelian property means that it does not matter in which order the updating rules are applied to the positions x. A proof of this can be found in [20].
In this work I implemented the OSM dynamics by performing the following steps:

1. Initialize a table with length L such that $H(x) = 2(L - x + 1)$.
2. Initialize $\eta(x)$ for each x
3. DO in time T:
   (a) Drive(pile)
   (b) As long as stability is not reached: Relax(pile), Update(stability)
   (c) After some time $T_{buff} < T$: Perform measurements on the system

T_{buff} serves as a buffering time which the simulation requires in order to reach its attractor (critical point) in phase space.

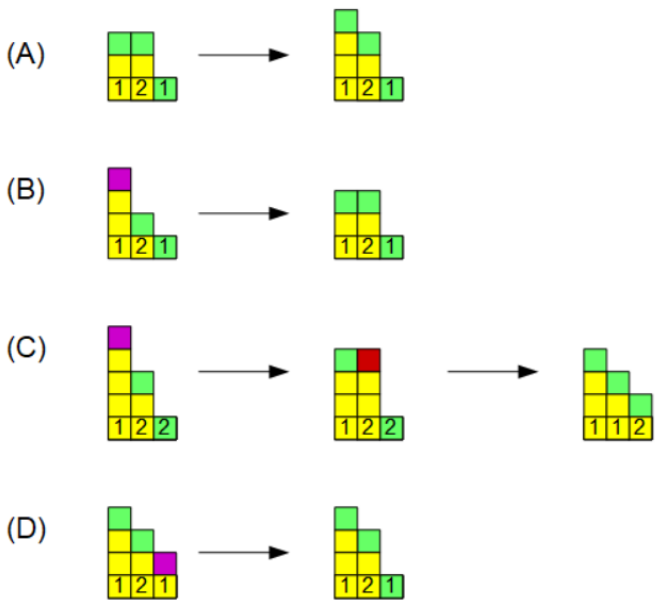

Figure 4: Dynamical rules for updating the OSM. Shown is the profile of various $L = 3$ sandpiles. On the ground level $\eta(x)$, the local stability, is shown. The highest grain at position x carries a colour indicating its stability: (green) stable, (violet) unstable with probability p and (red) unstable. 4 distinct situations are presented: (A) a grain is added, (B) a grain drops and becomes stable, (C) a grain drops two steps, the value of $\eta(x = 2)$ changed by chance while $x = 2$ toppled and (D) a grain leaves the system.

2.4 Behaviour at the critical point

The main result of the Oslo model is the fact that the distribution $p(s)$ of the size of toppling events features a power law with exponential cut-off. Unlike the experiment in [9] however, the exponent $\tau \approx -1.53$, not -2. Also the cut-off is not observed. In order to connect the findings to equilibrium criticality, the scaling function $\mathcal{G}$ is introduced:

$$p(s, L) \propto s^{-\tau} \mathcal{G}\left(\frac{s}{s_c}\right) \quad , \tag{2.3}$$

$$s_c(L) \propto L^D \quad . \tag{2.4}$$

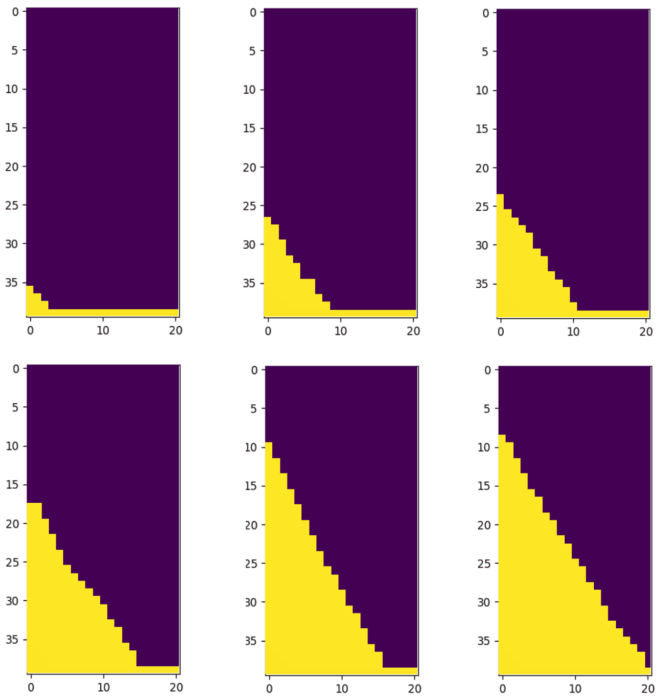

Figure 5: 6 frames taken from the simulation while building up and reaching the attractor configuration. $L = 21$.

In the steady state it is assumed that the inflow $M_{in} = 1$, balances approximately the outflow $M_{out} = \langle s \rangle / L$. By simply requiring $\langle s \rangle \propto L$ a scaling relation can be found [19]:

$$D(2 - \tau) = 1 \qquad . \tag{2.5}$$

As criticality can only lead to fractional critical exponents, the exact form of τ and D is often conjectured to be $\tau = 14/9$ and $D = 9/4$.
Interestingly this observation is quite stable for any choice of the stability parameter p. Quantities like the height or total potential energy of the sandpile, which will be discussed in further depth below, however change. A high value of p for instance leads to sandpiles of lower height. We observe the interesting phenomenon that, while their average changes significantly, dynamics in vicinity of the steady state remain the same.

3 Sandpiles As Thermodynamic Systems

Similar to the Ising model for equilibrium critical systems, the OSM could be considered a benchmark model to study SOC. But unlike the Ising model the critical behaviour of the Oslo model is mainly understood by computational methods. Only for systems of very small size L ([20], [21]) or in the continuum limit [22] exact analytic results are known. In the following I will collect some observations which will help to establish a statistical understanding of the Oslo model using the route of SSR processes.

3.1 Macrostates of the OSM

Energy and mass

Knowing $H(x)$, the potential energy and mass can be easily derived: Mass is equal to the sum over heights,

$$M = \sum_{x=1}^{L} H(x) \quad , \tag{3.1}$$

and energy is the sum of local potential energies,

$$E = \sum_{x=1}^{L} \frac{H(x)H(x+1)}{2} \quad . \tag{3.2}$$

The minimally stable configuration, e.g. a pile with surface $k(x) = 1$ for all x, has energy E_{min} and mass M_{min}:

$$E_{min} = \frac{L(L+1)(2L+4)}{12} \quad , \tag{3.3}$$

$$M_{min} = \frac{L(L+1)}{2} \quad . \tag{3.4}$$

The maximally stable surface ($k(x) = 2$ for all x) features an energy E_{max} and a mass M_{max}:

$$E_{max} = \frac{L(2L+1)(4L+4)}{12} + \frac{L(L+1)}{2} \quad , \tag{3.5}$$

$$M_{max} = L(L+1) \quad . \tag{3.6}$$

It holds that

$$\frac{E_{min}(2L) + L(L+1)}{2} = E_{max} \quad .$$

Other measures

Throughout the thesis I will also analyse further measures that capture information about the structure of a surface.

1. Slope frequencies n_0,n_1 & n_2: Local slopes with $k(x) = i$ will be observed n_i times in a certain sandpile. For any stable configuration one finds $n_r = 0$ with $r > 2$. The slope frequency n_2 therefore is the number of times a site x has $H(x-1) - H(x) = 2$ in a given surface.

2. Surface length φ: If we conceive the surface of the sandpile as a curve in $\mathcal{N}^2$, the tuple $(k(x), 1) = (\Delta H, \Delta x)$ is describing a local discrete derivative. Forming the norm gives an estimate for the local length of the surface at these positions x,

$$\varphi = \sum_{x=1}^{L} \sqrt{k(x)^2 + 1} \qquad . \tag{3.7}$$

3. Load κ: If a grain is moved n steps to the right, this measure of the pile exactly reduces by its distance travelled. If we start with an empty table and add grains reversely from the boundary and push them to the origin, then $\kappa = 1$ refers to a single grain laying at $x = L$. Pushing it to the left increases κ. Generally κ counts the number of pushes we had to apply in total in order to arrive with the given configuration. Mathematically this can be derived by a simple sum,

$$\kappa = \sum_{x=1}^{L} H(x)(L - x + 1) \qquad . \tag{3.8}$$

4. Average slope α: It can be calculated by a linear fit through the height profile. For this purpose the least square displacement was used. Given some data x and $y(x)$ the linear fit, that minimizes the squared error, has a slope of α_{LS},

$$\alpha_{LS} = \frac{L\sum(xy) - \sum(x)\sum(y)}{L\sum(x^2) - (\sum x)^2} \qquad .$$

   Applied to our problem this gives

$$\alpha = 6 \cdot \frac{2\kappa - (L+1)M}{L(L^2-1)} \qquad . \tag{3.9}$$

   The formula is applicable as $L > 1$. One can test that plugging in the minimally possible mass and load, gives $\alpha = 1$.

Without much of an influence on the result we may also wish to perform the least squares fit with the additional condition of $H(L+1) = 0$. Then α_{LS} reduces to (see eg. [23])

$$\tilde{\alpha}_{LS} = \frac{\sum(xy)}{\sum(x^2)} \approx \frac{3\kappa}{L^3} \quad ,$$

which yields a direct proportionality to the defined load κ,

$$\tilde{\alpha} = 6 \cdot \frac{\kappa}{L(L+1)(2L+1)} \quad . \tag{3.10}$$

In this way a physical interpretation to the abstractly defined load is found.

5. Approximated height $H'(1)$: Extrapolating the line with mean slope to $x = 1$ gives a measure for the height of the pile,

$$H'(1) = \alpha L \quad . \tag{3.11}$$

It is to expect that $H(1) \approx H'(1)$. If $\Delta H = H(1) - H'(1)$ is negative, then the surface is rather curved outwards.

6. Approximated quantities E', M', κ' & φ': Assuming such a linearised pile, we can go further and ask, how much energy or mass a sandpile with mean slope α contains. These quantities are derived to

$$M'(L) = \int_0^L \left(H'(1) - \frac{H'(1)}{L} x \right) dx = \frac{H'(1) \cdot L}{2} \quad , \tag{3.12}$$

$$E'(L) = \int_0^L \frac{H'(x)^2}{2} dx = \frac{H'(1)^2 \cdot L}{6} = \frac{H'(1) \cdot M'}{3} \quad , \tag{3.13}$$

$$\kappa'(L) = \int_0^L \alpha \cdot x^2 \, dx = \frac{\alpha \cdot L^3}{3} = \frac{H'(1) \cdot L^2}{3} \quad , \tag{3.14}$$

$$\varphi'(L) = L\sqrt{\alpha^2 + 1} \quad . \tag{3.15}$$

3.2 Microstates of the OSM

During the course of a simulation different macrostates X_i will be reached. For the purpose of further discussions I would like to introduce a nomenclature in order to distinguish the sets of driven $\mathcal{D}$, unstable $\mathcal{I}$, stable $\mathcal{S}$ and meta-stable $\mathcal{M}$ states. The union of stable and meta-stable states is referred to as the set of recurrent configurations: $\mathcal{R} = \mathcal{M} \cup \mathcal{S}$. A driven state gets defined as a state that was reached directly after a driving event (the grain gain at $x = 1$). A meta-stable state is a state which is only stable with a probability, due to $\eta(x)$. Figure 6 shows a sketch of those sets.

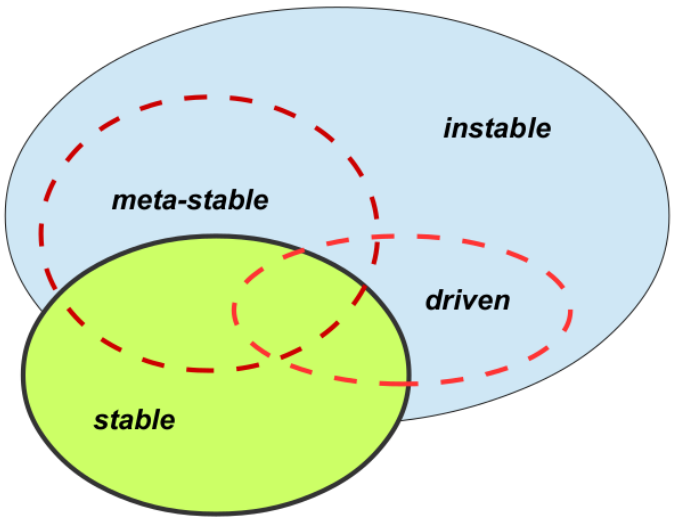

Figure 6: A sketch of the defined sets of micro configurations: driven $\mathcal{D}$, unstable $\mathcal{I}$, stable $\mathcal{S}$ and meta-stable $\mathcal{M}$. Stable states are never unstable. Driven and meta-stable states can however be stable or unstable depending on the underlying structure of $\eta(x)$

It is important to note that, depending on the choice of set and analysed macro variable, we will also find different distributions and dynamics. For small pile sizes the exact dynamics can be still computed analytically. Given for instance the energy E, a sandpile of size $L = 2$ and the set of all reachable states, each energy can be conceived as a state in a Markov chain. A colour-coded form of the corresponding transition matrix is shown in figure 7.

Enumeration of the recurrent states in $\mathcal{R}$

To find the number N of recurrent states one can proceed as described in [24]. Lets adopt the slope-formulation of the sandpile. States can have slope 0, 1 or 2. The foot of the sandpile can either have slope 1 or 2. In the neighbouring

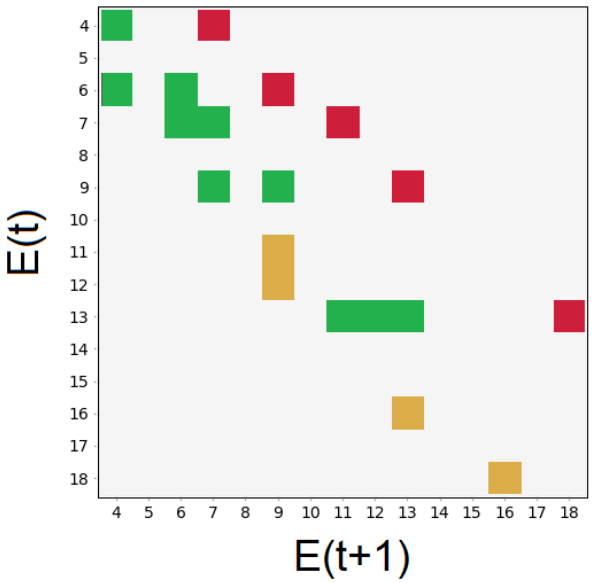

Figure 7: The color-coded adjacency matrix of a Markov chain model of the Oslo sandpile. Matrix elements correspond to energies measured on the set of all reached states in the sandpile of size $L = 2$. Green: Stable or meta-stable, Yellow: Instable, Red: Driven. There are 5 stable energy levels, but 9 reachable energy levels in total.

position the possible slopes depend on the slope in the position to the right. By looking at the dynamics one realizes that in a recurrent configuration the slope 2 can be followed by all slopes, but 1 only by 1 or 2. A slope 1, lets call it 1_2 that was proceeded by an arbitrary amount of slopes 1 and one slope 2, can however be followed by slope 0. We have to distinguish two forms of slope 1: 1_0 and 1_2. The one that was proceeded by ones and a zero, and the one that was proceeded by ones and a two. 0 can always be followed by 1_0 and 2. "Followed" in the sense that the position to the left is in that state. Figure 8 visualizes these rules as a directed graph.
To formalize, lets call $N(k(1), L, h(1))$ the amount of states N of a pile with slope state $k(1)$ and active height $h(L)$ at the top. We can then write recursively:

$$\begin{aligned} N(2,L,h) &= N(2,L-1,h-1) + N(1_0,L-1,h-1) \\ &\quad + N(1_2,L-1,h-1) + N(0,L-1,h-1) \quad , \\ N(1_0,L,h) &= N(1_0,L-1,h) + N(0,L-1,h) \quad , \\ N(1_2,L,h) &= N(1_2,L-1,h) + N(2,L-1,h) \quad , \\ N(0,L,h) &= N(2,L-1,h+1) + N(1_1,L-1,h+1) \quad . \end{aligned}$$

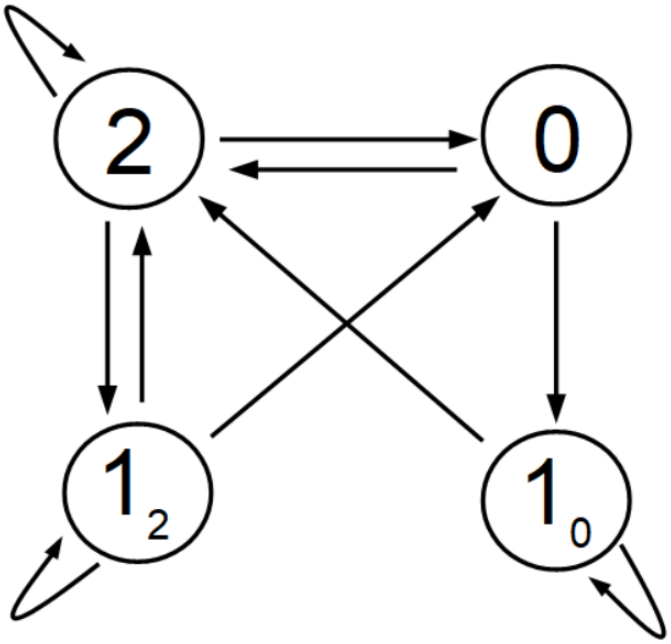

Figure 8: A generating graph for stable configurations of the system. The nodes symbolize slope values $k(x)$. Moving along a link gives all possible preceding slope values $k(x-1)$. By moving over all possible paths, given the initial condition $k(L) \in \{1_0, 2\}$, the number of configurations can be enumerated.

From this, one can obtain a recursive relation, by integrating with respect to h and the slopes,

$$N(L) = 3N(L-1) - N(L-2) \quad .$$

This recursive relation is a relative to the generator of the Fibonacci series and can be solved by setting $N(x) = \lambda^x$,

$$\lambda_{1,2} = \frac{3 \pm \sqrt{5}}{2} \quad .$$

We have initial conditions $N(1) = 2$ and $N(2) = 5$. Therefore the number of recurrent states of a pile of size L is equal to

$$N(L) = \frac{2+\sqrt{5}}{\sqrt{5}} \lambda_1^{L-1} + \frac{\sqrt{5}-2}{\sqrt{5}} \lambda_2^{L-1} \quad . \tag{3.16}$$

The number of recurrent configurations is growing exponentially. This large increase in state space and complexity explains why there is up to date no

analytical understanding of sandpiles with large system size. [20] offered a recursive relation for the transition matrix. Its form however quickly becomes untraceable for large systems. The aim of this thesis therefore will not be an analytical understanding but a statistical one.

Multiplicity of energy and mass states

With reference to figure 8 we can't only enumerate all recurrent configurations X_i, but also compute the energies E_i, masses M_i & heights $H_i(1)$ of specific surfaces. This I did for some selected macro variables with the help of a computer. By moving over all possible paths in the figure from $k(L)$ to $k(1)$ given the initial condition $k(L) \in \{1_0, 2\}$ the exact shape of all X_i can be obtained. Using Eq. (3.2) & Eq. (3.1) the energies and masses are then computed. As the $E_{max}(L) - E_{min}(L)$ grows way slower than $N(L)$, it is clear that the majority of energy states E_i will be degenerate. Same holds for mass and height. Counting all states can only be performed for small sandpiles. We can however extend sampling to systems of larger size, by Monte Carlo simulation. We initiate a set of random walkers on the graph in figure 8 and let them diffuse randomly. For this purpose it was assumed that given a node in the network, any available link from that node to another one is chosen with equal probability. The set of resulting trajectories can be used to find estimates for the multiplicities, q, of $H(1)$, E and M.

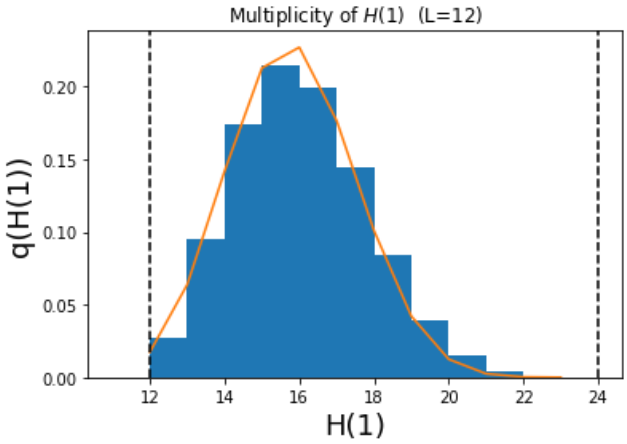

Figure 9: For a small sandpile the multiplicities of height H can be computed explicitly. Shown is the level of degeneracy of different height levels $H(1)$ given a pile of size $L = 12$. Dotted lines indicate the theoretical boundaries to the measure as calculated with Eq. (3.17).

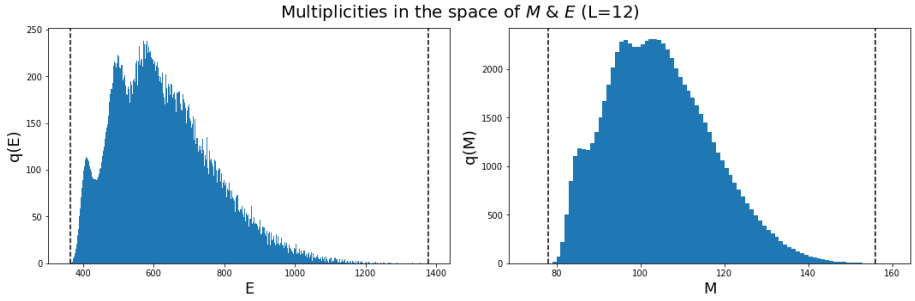

Figure 10: Same pile-size as in 9, but for mass and energy. It is interesting to observe that the distribution shows a polymodal structure.

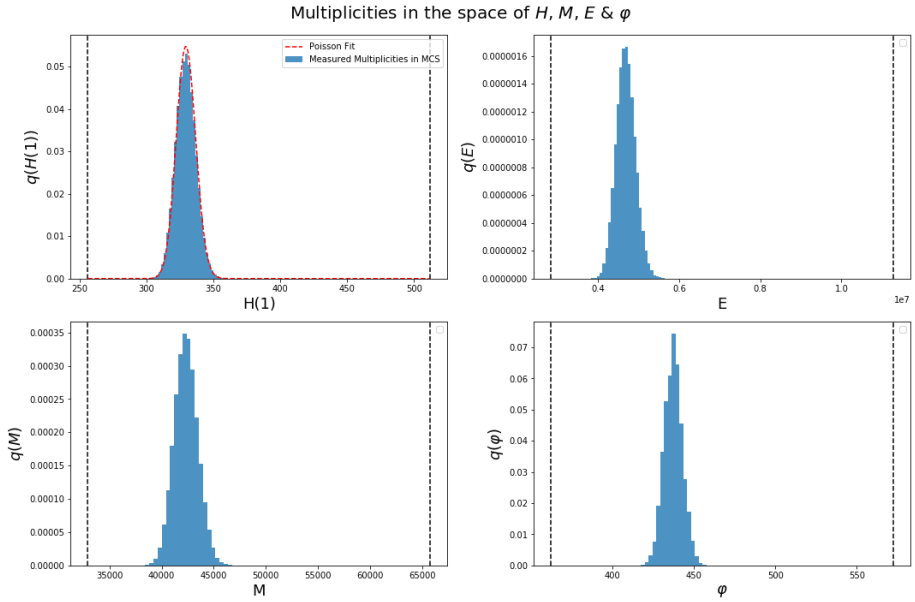

Figure 11: Results of Monte Carlo simulations performed on the generating network shown in figure 8. Shown are 4 chosen macro variables: height, mass, energy and surface length. The dotted lines indicate the theoretical boundaries.

.

Simulations suggest, that the limiting distribution of random walkers and thus our expected relative multiplicity for $H(1)$ can be approximated by a Poisson distribution, which takes a Gaussian shape for large L as a result of the central limit theorem,

$$q(H(1)) \sim \frac{1}{\sqrt{2\pi\mu_H}} e^{-(H(1)-\mu_H)^2/2\mu_H} = \mathcal{N}(\mu_H, \mu_H) \qquad . \tag{3.17}$$

Expected multiplicities, q, of mass and energy can be approximated from $p(H(1))$ by assuming that the pile has a linear slope,

$$q(M) \sim \mathcal{N}(\frac{L\mu_H}{2}, \frac{L^2\mu_H}{4}) \qquad , \tag{3.18}$$

$$q(E) \sim \sqrt{\frac{3}{4\pi L^3 \mu_H E}} e^{-3\left(\sqrt{E}-\sqrt{\mu_H^2 L/6}\right)^2/L\mu_H} \qquad . \tag{3.19}$$

It is important to note that the value of the average height, μ_H, and all other constants will change significantly if the transitions probabilities to jump from one node to another in the graph are altered. This will be exactly the situation once we introduce the toppling probability, p, entering in $\eta(x)$.

3.3 The attractor configuration

We will first study the attractor dynamics by studying its compositions n_1,n_2 and n_0. By understanding these compositions it will be further on possible to derive expectation values of other macro variables. Given a certain pile of length L and local toppling probability p, can we compute the expected value of n_2 of the attractor configuration?
We define the mean probability to find a slope of $k = i$ as p_i. In order to estimate p_i, simulations were performed of a sandpile of length $L = 100$ and varying p. Figure 12 shows the results for the average of $p_i = n_i/L$. Note that p_i are not fixed and can change over the course of a simulation.
Let us highlight 3 observations: (1) While n_2 decreases with p, n_1 increases at almost the same rate. (2) The number of flat slopes n_0 is relatively low for most values of the parameter p. (3) The global toppling probability p_g, which we define to give an estimate for the chance that a randomly chosen position x is going to topple if a grain drops on it, does not change drastically and is around 0.9. p_g consists of the probability to find a slope 2 at any position x, p_2 (which would topple with certainty in case of an avalanche hitting it) and the probability of a newly formed slope of 2 to become unstable once loaded, $p \cdot p_1$. We set the global toppling probability as

$$p_g = p_2 + p \cdot p_1 \qquad . \tag{3.20}$$

p_g is relatively robust under variations of p (see figure 12). This is a prerequisite for the avalanche probability to be universal for many different choices of p.

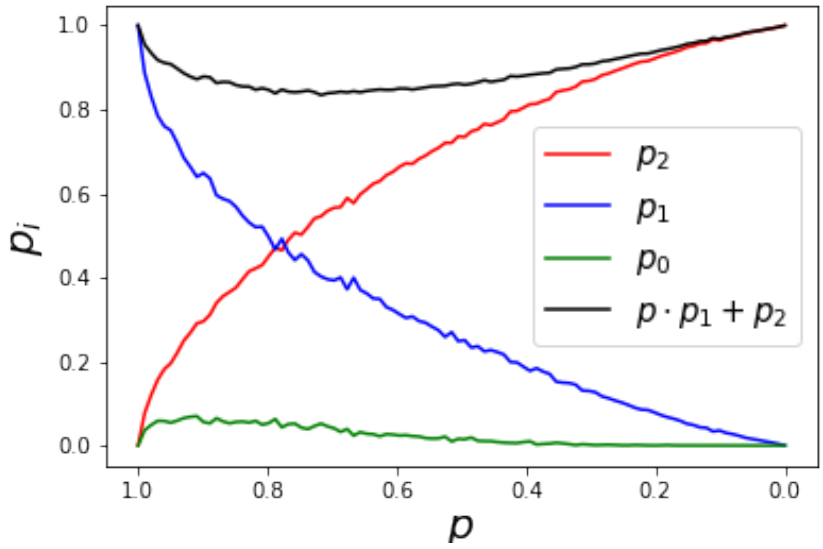

Figure 12: The butterfly like shape shows the mean chance of finding n_i slopes $k = i$. With decreasing toppling probability the chance of finding a slope of 2 increases. Rather in a similar manner p_1 decreases. The average chances of finding a flat slope are rather low. Also shown is the value of the global toppling probability p_g as a function of the local toppling probability defined in Eq. (3.20).

3.4 Correlations of macrostates

An ideal gas can be described by measures, such as pressure and temperature. By performing multiple experiments, it is observed that the gas suffices Gay-Lussac's Law $P \propto T$. In a similar way we can ask, which are the correlations among macrostates of the Oslo model?

Correlations of macrostate positions in phase space

An idea for the mean correlations can be already deduced from the linearised pile. For instance it is to expect that $E \propto H(1) \cdot M/3$. The whole accessed phase space is however a lot richer and trajectories of M and E move in it. We study this situation with the help of 2D-histograms (figure 13]).
Let us collect a few observations:

- Energy and load are strongly correlated.
- Mass and energy are correlated, but allow for a larger variance.

- The surface length is only loosely correlated with M, E and κ in a non-linear way.
- The theoretical boundaries (eg. E_{min}, E_{max}) are not reached. We expect this from the study of multiplicities.

In the following we want to focus on the dynamics of M and E. First we will survey the boundaries of the M-E phase space by invoking some theoretical considerations (figure 14), then take a closer look at the internal dynamics.

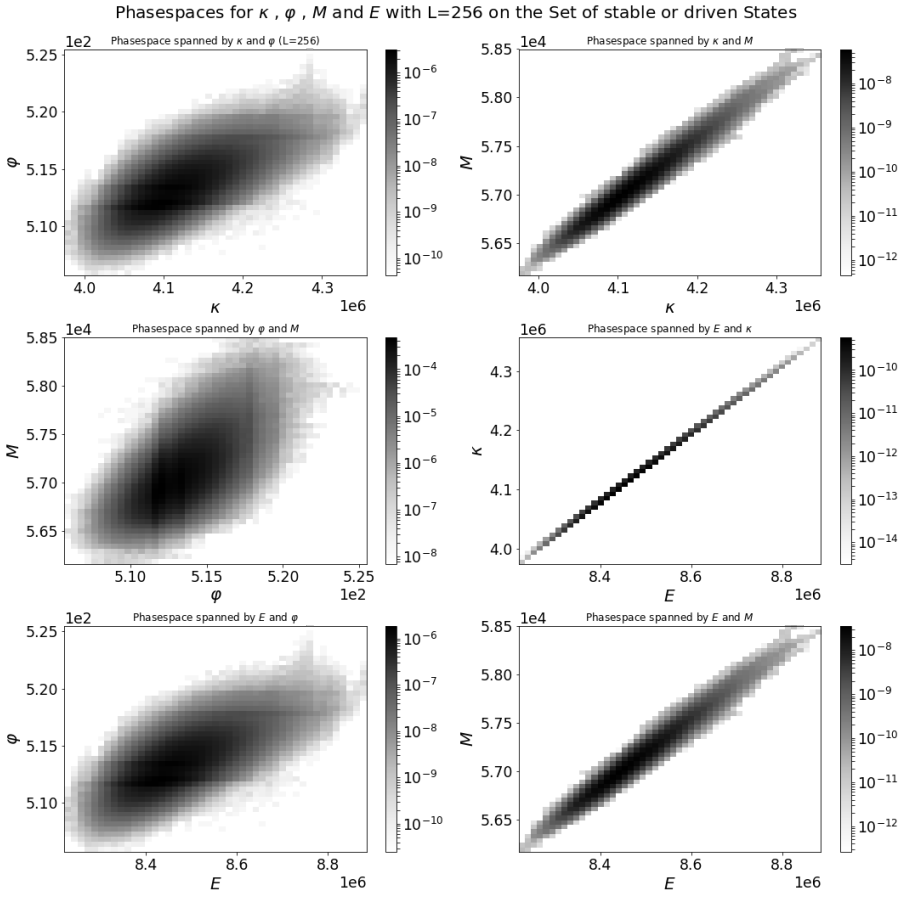

Figure 13: Phase spaces spanned by load κ, surface length φ, mass M and energy E. Energy, mass and load are linearly dependent. Configurations of a given surface length can have however multiple energies and E increases with φ in a nonlinear way.

In figure 14 it is observed that the linear sandpile of minimum height (violet line) is in fact almost never realized. However, the mimimum value of $H(1)$ is realized with "superlinear" values of $E > E'$, such that we can deduce from those observations that the surface of the sandpile of lowest height is curved outwards. Linear surfaces with the average height are only realized for the smallest observed energies. Conversely sandpiles with linearly shaped slope of maximum height are only populated by the highest energies. In other words, sandpiles of maximum height have at most a curvature of 0, but may be negatively curved. The dynamics happen between the red and green line, linear sandpile surfaces respectively. More can not be said at this point, but we keep in mind that high sandpiles are rather curved negatively, while low heights indicate outward curved surfaces.

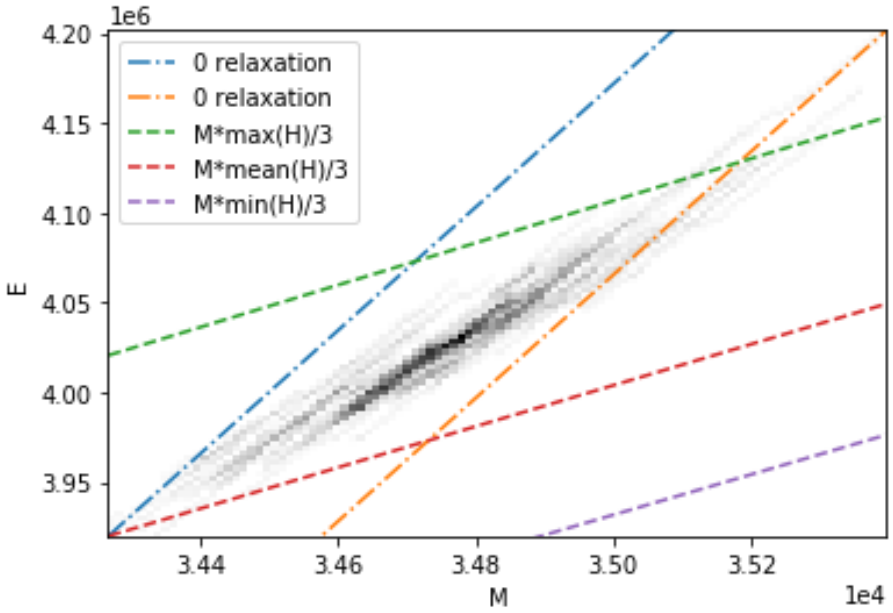

Figure 14: Phase space spanned by mass and energy. Further shown are linear approximations $E' = MH(1)/3$ at different fixed heights: The highest, lowest and mean observed height $H(1)$. The lines "0 relaxation" indicate the curves with slope $dE/dM = H(1)$, which correspond to the idealized extreme dynamics where the sandpile would not loose any grains but is continuously driven.

Correlations of phase space dynamics

In the introduction I mentioned that driven dissipative thermodynamic systems can potentially be described on the macrolevel by partial differential equations. In order to study the dynamics we will look at the mean movement of a phase-space increment on the set of all states, including transient states $\mathcal{I}$. $\mathcal{I}$ has to be included as relaxation steps are too large otherwise, such that they can not be visualized properly. In the space of M and E the mean increase or decrease of energy $\langle \Delta E \rangle (M, E)$ was computed,

$$\langle \Delta E \rangle (M, E) = \sum_{\Delta E} \Delta E \; p(\Delta E \mid M, E) = \sum_{\Delta E} \Delta E \; \frac{p(\Delta E, M, E)}{p(M, E)} \qquad . \quad (3.21)$$

Using this and similarly $\langle \Delta M \rangle (M, E)$, a dynamical vector of the average dynamics at a given point in phase space is known. Then simulations were performed. Some particular results can be seen in figures 15-18. Arrows are normalized. The directionality of such average vectors can only indicate normalized averages over many realizations of the dynamics.
Note that the depicted flow-patterns connect to the general expectations about the driven non-equilibrium steady state mentioned in the introduction. The dynamics are not confined to a point or a cloud in phase space. Macro variables perform cyclic stochastic movements. As these emerge in the long term limit of the sandpile dynamics we can refer to them as stochastic limit cycles. Sandpile dynamics, and probably driven non-equilibrium systems in general, have non vanishing average net flows through their phase space. In particular the system is never in detailed balance.

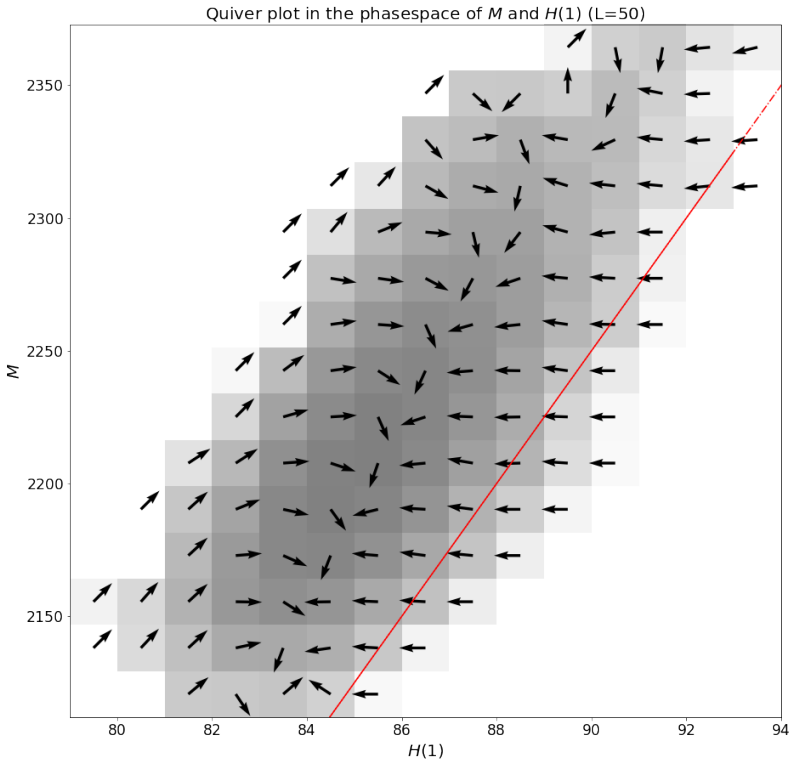

Figure 15: Dynamics in the phase space spanned by $H(1)$ and M. The red line indicates the linear pile $M = HL/3$. Mass is therefore mostly acting in a superlinear regime. This means that observed sandpiles with a height H have higher mass than a theoretical sandpile which features a linearly increasing profile from 0 to H. High sandpiles of linear shape quickly loose the peak around $x = 0$ and the height decreases away from the red line. If avalanches are large enough, the channel in the center of the structure is hit and grains can drop out of the system, allowing for further reductions in the height. If the mass is relatively large compared to the height, this indicates a outwards curved surface, which offers a shallow plateau onto which new grains can be dropped, such that the height an mass grows.

.

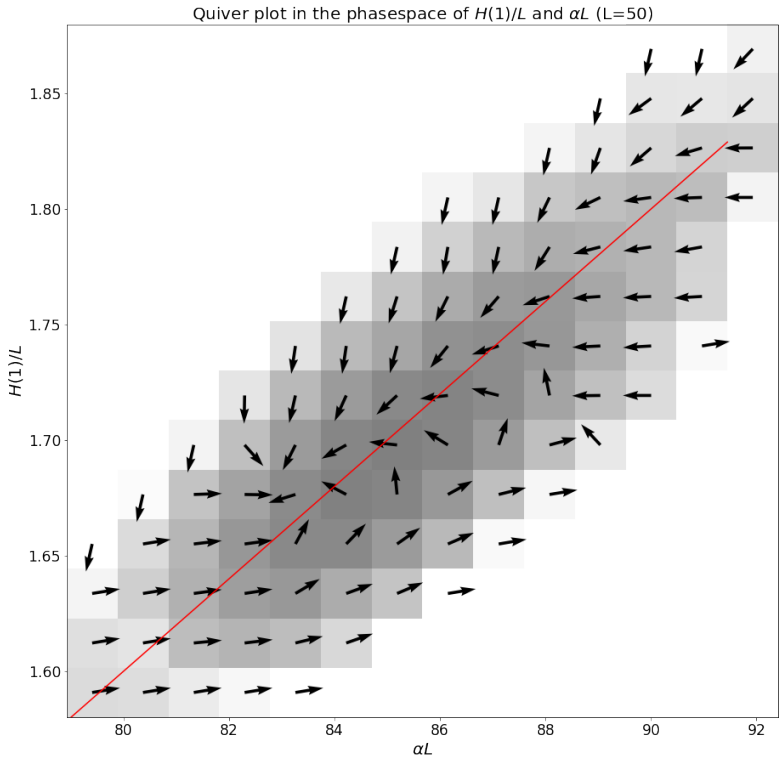

Figure 16: Phase space spanned by height $H(1)$ and the height as estimated with the help of the slope αL. Further shown is the line of reflection. $H(1)$ was rescaled by $1/L$ to match average transition sizes of both measures. The plot appears to feature a stochastic cycle in the curvature. Note that any state above the red line is associated with a inwards curved surface, while staes below the red line are rather curved outwards. High sandpiles will collapse and reduce the height above the red line. A relaxed surface offers more capacity to carry grains, such that any addition of grains is quickly redistributed from the peak to the remaining surface (the red line is crossed to the left for small heights). At some point grains can not be redistributed any more and the peak builds up again below the red line.

.

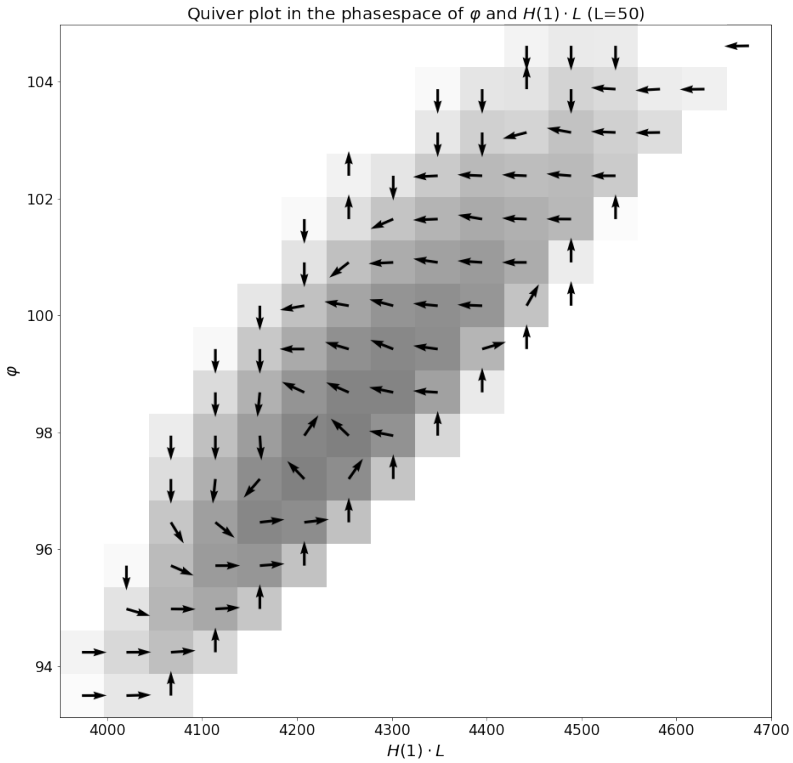

Figure 17: Phase space spanned by surface length φ and the height $H(1)$. The plot is related to figure 16. Outward curved surfaces can be reduced without changing the top height of the pile considerably by ejecting mass. Then the pile builds up again, gaining surface and height reaching a inwards curved regime. Then the height is reduces, while the surface length remains more or less constant, as mass does not leave the system and is mainly redistributed (see. section 4.9). We have again arrived at the initial outwards curved regime

.

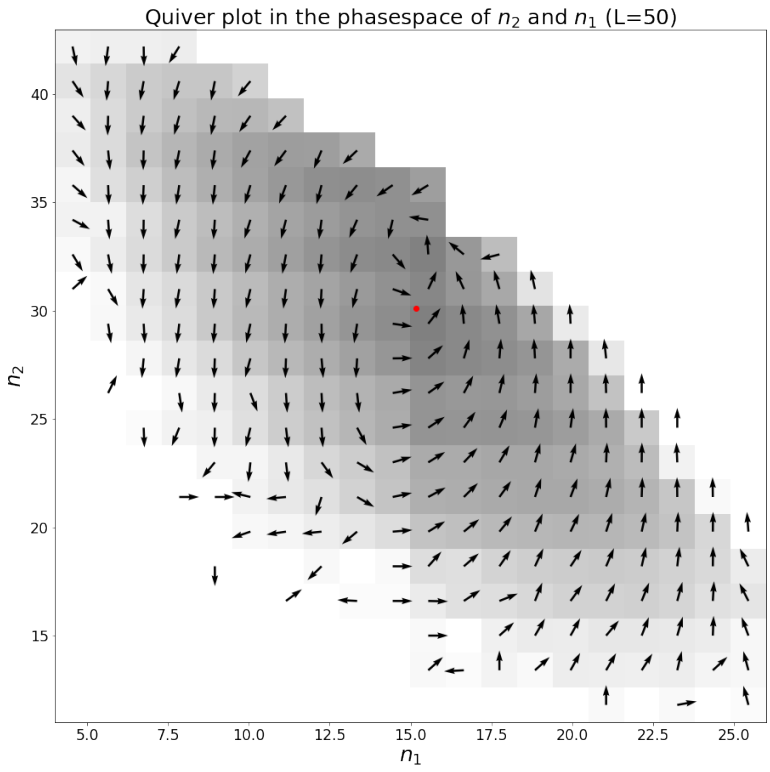

Figure 18: Phase space spanned by surface length n_2 and n_1. The red dot indicates the mean $(\langle n_1 \rangle, \langle n_2 \rangle)$. Perhaps the most convincing limit cycle is found in this space revolving around the mean. Sandpiles with high n_1 will grow and increase the height by adding slopes of 2 (right side). As n_1 remains rather constant in this process, the increase in n_2 mostly comes from saturating slopes of 0. As n_0 is associated with being outward-curved, we can again identify this growth face with a transition towards an instable high peak. Next the peak collapses, and some grains will halt at a slope 1, effectively decreasing n_1, while increasing or conserving n_2. A outward-curved belly forms. Eventually the whole belly breaks away in a large avalanche leaving the system in stable, low energy, state.

4 Sample Space Reducing Processes

Most of equilibrium thermodynamics is concerned with systems, whose phase space Ω is fixed for a given set of extensive parameters (eg. volume V or particle number N). Take for example a piston filled with gas, on which we exert a force. Such a process will change the chances according to which a particle inside will be found having a certain energy state s. If we see the particle as a system connected to a heat bath constituted by the multitude of interactions with its neighbours, we can quantify the situation within the framework of the canonical ensemble. Then we expect the probability to be of exponential form,

$$p(s) = \frac{e^{-\beta s}}{Z} \quad . \tag{4.1}$$

Z being the partition function and β being an equilibrium quantity, typically $\beta = 1/k_B T$.
Within the conception of statistical inference this exact functional form of Eq. (4.1) can be obtained by minimizing the Shannon entropy functional S in Eq. (1.2) with the constraint of having a fixed expectation $E(s)$.
In the described situation the overall sample space of reachable particle energy levels did not change. Generally the particle will have the freedom to change to higher and lower levels of excitement. However what can we say about a process in which this freedom is constrained?
Corominas et al. [25] proposed a simple framework, which they named Sample Space Reducing processes (or short SSRP). It was successfully used to explain the statistics of undirected network graphs ([26]), cosmic particles ([27]) and statistical patterns in language ([28]).
This chapter will begin with the description of the simplest such SSRP, namely the "slowly driven" SSRP. Then this concept will be extended by tweaking the prior probabilities, the driving rate, the type of driving and the transition probabilities. With each extension of the SSR framework further observations that emerge from the dynamics of the Oslo model can be modelled. By the end of this chapter I will make the connection to the Oslo model quantitative, by characterizing the underlying SSRP in terms of the macro variables defined in chapter 3.

4.1 Slowly driven SSR processes

Consider a process acting on the states of a system in such a way, that the energy can only be reduced (i.e. a hot system in contact with a cold heat bath). Once the ground state of the system is reached the process restarts again at a random state (i.e. by coupling to a hot heat bath).
The situation can also be illustrated using dice ([25]). Let our system span the space of natural numbers and we set the current state to $i = 11$ for example. As all states below 11 will be reachable in the next step of the process, the current sample space size $\Omega_1 = 10$. Then we throw a 10-sided dice to recover the state following the first jump j. Similarly a dice with $\Omega_2 = j - 1$ sides will decide

the state following the second jump and so forth until the state $i = 1$ is reached and the process is restarted by driving it to a random higher state. The highest state is dictated by the system size W.
An alternative narrative would be one of a ball jumping down a staircase. Due to gravity and its momentum the ball will not jump back upwards. This is illustrated in figure 19.

In all these situations the sample space, $\Omega = \Omega_t$, is a function of time t and is

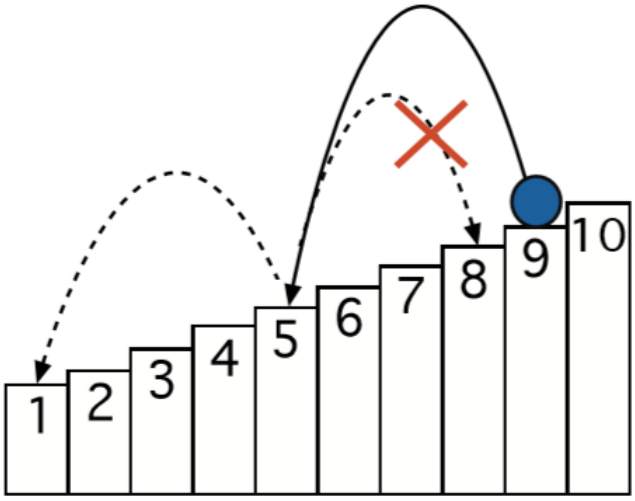

Figure 19: A ball falls down a staircase and can never jump back upwards but will reach all steps below with equal probability. Once the ball has reached the lowest level, we iterate the process with a new ball. Figure taken from [25].

strictly reduced,

$$W \supset \Omega_1 \supset \Omega_2 \supset \cdots \supset \{1\} \quad .$$

Mathematically the situation can be realized by a Markov chain with the following transition matrix:

$$p(j \mid i) = \begin{cases} \frac{1}{i-1} & i > j \\ \frac{1}{W} & i = 1 \\ 0 & \text{else} \end{cases} \quad . \tag{4.2}$$

This matrix is further visualized in figure 20. The transition probability of $1/(i-1)$, given initial state i and terminal state $j < i$, is not the only possible realization of a SSRP. Due to its uniform character we may refer to it as "micro-canonical".
From the theory of Markov chains we can then try to solve the master Eq. (4.3) in order to characterize the attractor configuration of the system and henceforth

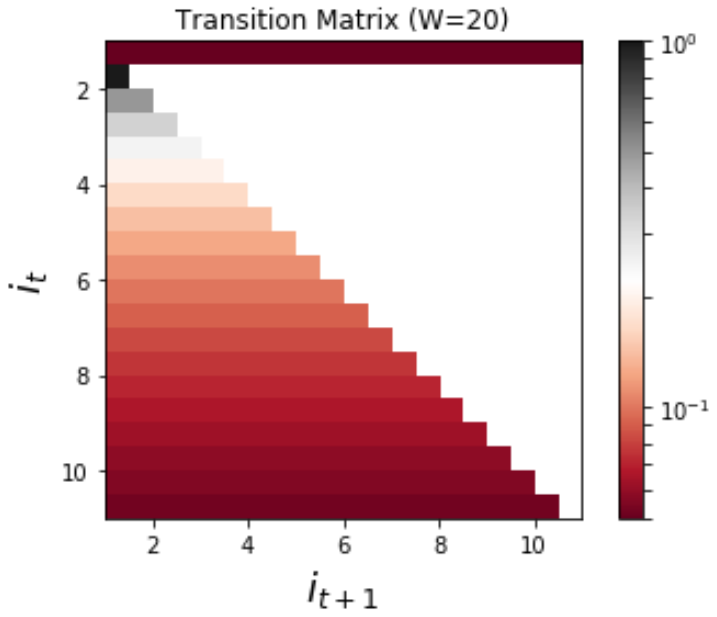

Figure 20: A color coded transition matrix to visualize the structure of Eq. (4.2).

the marginal probabilities $p(i)$ of finding the system in a certain state i at any moment,

$$p(i) = \sum_{j=1}^{W} p(i \mid j) \cdot p(j) \qquad . \tag{4.3}$$

As [25] have shown, the probabilities follow a power law of exponent -1, also often referred to as Zipf's law,

$$p(i) = p(1) \cdot \frac{1}{i} \qquad . \tag{4.4}$$

$p(1)$ is given by the normalization condition,

$$p(1)^{-1} = \sum_{j}^{W} \frac{1}{j} \qquad . \tag{4.5}$$

I will quickly sketch the logic of the proof. We start with Eq. (4.3). Since we are dealing with a SSRP, it is legitimate to start the sum at $j = i + 1$ instead of $j = 1$. Then we form the difference $p(i + 1) - p(i)$;

$$p(i+1) - p(i) = \sum_{j=i+2}^{W} p(j)p(i+1 \mid j) - \sum_{j=i+1}^{W} p(j)p(i \mid j) \qquad .$$

Applying the specific form of the transition probabilities in Eq. (4.2), we find

$$p(i+1)(i+1) = p(i)i \qquad .$$

Equation (4.4) is the general solution to this relation.

The result is in agreement with simulations (see figure 21). Computationally I used three methods to arrive at the attractor configuration: (1) by consecutive multiplication of the transition matrix onto a random normalized initial configuration, (2) by performing a Monte Carlo simulation of a ball walking stochastic on such a landscape, depicted in figure 19, and (3) by computing the largest eigenvalue of the transition matrix and its corresponding eigenvector (Perron-Frobenius eigenvector). The results of all three methods are consistent.
This form of SSR process is called slowly driven, as the process only restarts once it has completely relaxed to the ground state. So far the analysis has been rather ignorant towards the small timescale of individual relaxation processes and focused on the distributions recovered on a large timescale, spanning many cycles.

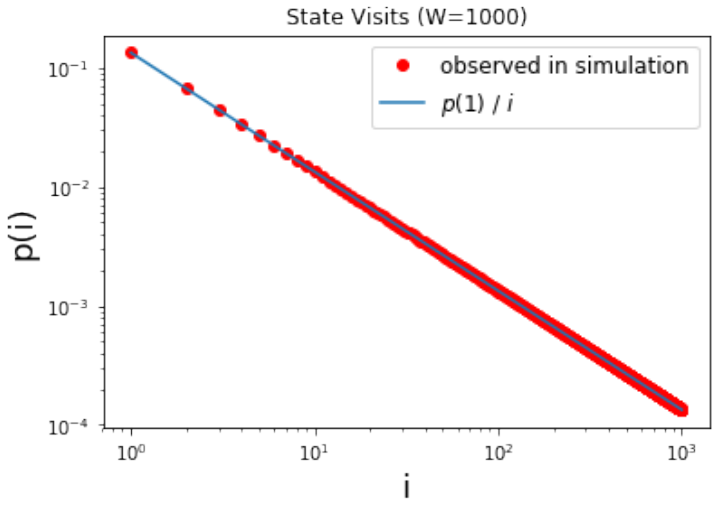

Figure 21: Comparison between the distribution of state visits recovered in simulations (red) and the theoretically expected Zipf distribution (blue).

Qualitatively one can see the Oslo model as a slowly driven SSR process. Also there the system is only driven once a stable state is reached by the process. By adding more complexity to the SSR dynamics later on, we will see that also further characteristics of the Oslo model can be captured.

4.2 Different faces of SSR processes

I would like to point out some properties of SSRPs that are related to the discussion in [25] & [29]. First it is interesting to note that the mean state $\langle i \rangle$ declines exponentially, as on average the state level is halved in each relaxation step. Therefore during relaxation the mean field model predicts

$$\langle i \rangle(t) \propto 2^{-t} \quad . \tag{4.6}$$

Secondly, while the process starts at state k, what is the probability to find a state i along the relaxation trajectory parametrized with time t? As shown in a preceding study ([30]) the distribution of such states takes approximately an exponential form,

$$p(i \mid t) \propto e^{-\gamma(t) \cdot i} \quad .$$

One can illustrate this observation with an example of moving particles penetrating a wall. Each time the particle collides with target particles along its trajectory in the wall, the particle looses kinetic energy. The sample space of accessible kinetic energies along the trajectory is therefore reducing. For such experiments it is a well known observation that the depth of penetration into the wall has an exponential form (compare for instance the law of Lambert-Beer for radiation). If a whole ensemble of particles hits the wall, and we wish to look instead at the distribution of kinetic particle energies regardless of their position, Zipf's law, Eq. (4.4), will be discovered again.
Figure 22 shows my investigations into the distributions of $p(i \mid t)$. I compared the observed distribution of states i - given a certain time t after restart - with a geometric distribution featuring a mean $\mu = 2^{-t}$. This μ was chosen following the logic of the mean field model, Eq. (4.6).

Thirdly the time it takes for a sequence of relaxation events to terminate, or the time it takes for the above discussed projectiles to dissipate their momentum, is Poisson distributed with mean $\langle \tau \rangle = \log(W)$. To see this let us first look at relaxation events with $\tau = 0$. This happens after the driving process if we pick a projectile from the random ensemble which already has zero energy. The chances for this to happen equal $1/W$ with W being the number of energies or states to choose from in the first place,

$$p(\tau = 0) = \frac{1}{W} \quad .$$

Then we look at events with $\tau = 1$. This is the case where a projectile of regardless energy ϵ looses all its momentum during the first collision. As the

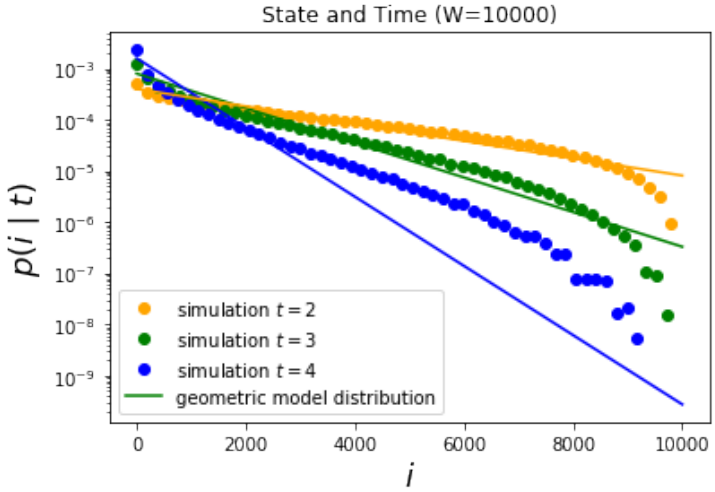

Figure 22: Comparison of the assumed geometric null model (with mean $\mu = 2^{-t}$, see Eq. (4.6)) for $t = 2, 3, 4$ steps, with the results obtained in simulations. The geometric distribution fits well for small t. SSRPs deviate from the model after a few relaxation steps. Nevertheless the decay remains exponential.

whole initial ensemble can perform such a relaxation we effectively need to integrate over all possible initial energies,

$$p(\tau = 1) \approx \frac{1}{W} \int_1^W \frac{1}{\epsilon} d\epsilon = \frac{\log(W)}{W} \quad .$$

If we then turn towards relaxations of length 2 we can start to construct a recursive scheme by integrating (A) all probabilities for particles having a certain residual energy ϵ after the first collision and (B) the chance that this energy ϵ is directly absorbed in the second collision,

$$p(\tau = 2) \approx \frac{1}{W} \int_1^W \log(\epsilon) \cdot \frac{1}{\epsilon} = \frac{\log(W)^2}{2W} \quad .$$

Following this scheme of successive integration recursively we arrive with the general form for $p(\tau)$:

$$p(\tau) = e^{-\log W} \cdot \frac{(\log W)^\tau}{\tau!} \quad . \tag{4.7}$$

This result is tested in simulations presented in figure 23.
Considering the wide range of distribution resulting from SSRPs, it is therefore of importance to be explicit about the quantity of interest when analysing such processes.

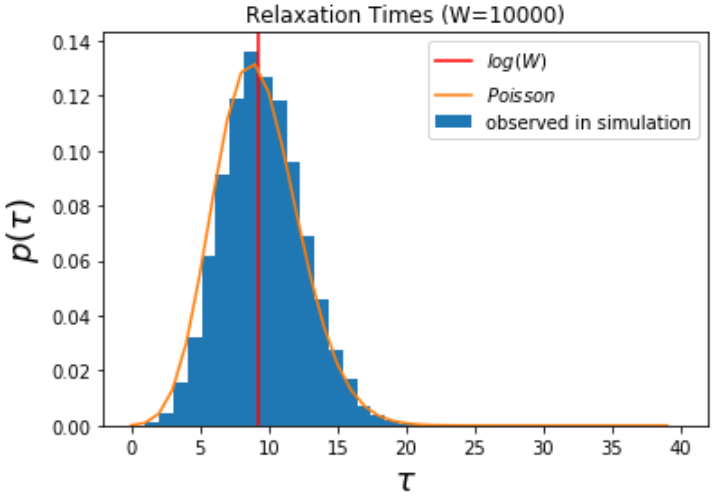

Figure 23: Simulations were run and the relaxation times, that is the number of steps starting from a random state until reaching the ground state, was recorded. The distribution is compared with a Poisson distribution with mean $\log W$ presented in Eq. (4.7). Both curves coincide well.

4.3 SSR processes with non-uniform prior probabilities

So far I repeated only the simplest possible case, namely a SSR process, with uniform prior probabilities, that is only restarted in the ground state. Lets first relax the first constraint and assume transition probabilities of the following form,

$$p(j \mid i) = \begin{cases} \frac{q(i)}{Q(i-1)} & i > j \\ \frac{q(i)}{Q(W)} & i = 1 \\ 0 & \text{else} \end{cases} . \tag{4.8}$$

Here $q(i)$ denotes the prior probability of state i and $Q(i)$ its cumulative distribution, $Q(i-1) = \sum_{j<i} q(j)$.

In order to visualize this process, one could think of SSR sequences of multi-sided dice, as illustrated before, but allowing the dice to have sides of different area. Also the staircase analogy might be helpful: It is a stair case process with non-uniform step size. The prior probabilities $q(i)$ are then proportional to the area of one step (figure 24).
By performing a similar ansatz as before, namely forming the master equation of the system and solving for its attractor distribution one arrives with the

following result for $p(i)$:

$$p(i) = \frac{q(i)}{Q(i)} \cdot p(1) \qquad . \tag{4.9}$$

This was shown in [26]. $p(1)$ follows from the normalization condition on p,

$$p(1)^{-1} = \sum_{i=1}^{W} \frac{q(i)}{Q(i)} \qquad . \tag{4.10}$$

One can now study different forms of prior distributions.

- For the case of $q(i) = 1/W$ we arrive with Eq. (4.4) as a result.
- For priors of polynomial form $q(i) = i^{\alpha}$ with $\alpha > -1$ Zipf's law remains the attractor for large systems. If the sample space is sufficiently large, it is safe to replace the sum occurring in Q with an integral. Therefore we have $Q(i) \propto i \cdot q(i)$ and $p(i) \propto i^{-1}$. This hints towards a certain robustness of the power law of power -1.
- Exponential prior probabilities $q(i) = e^{\beta i}$ with $\beta > 0$ however break the convergence to Zipf's law. Replacing the sum in Q with an integral predicts $Q(i) \propto q(i)$ and $p(i)$ being uniform. The exact form of $p(i)$ can be computed using limits of geometric series,

$$p(i) = p(1) \cdot \frac{1 - e^{-\beta}}{1 - e^{-\beta i}} \qquad . \tag{4.11}$$

- Looking at Eq. (4.11) and letting $\beta < 0$, we have a situation we may refer to as the SSR process in the canonical ensemble. If we expand $(e^u - 1)^{-1}$ into a Laurent series around $u = 0$ we actually find Zipf's law in first approximation. Therefore, as long as βi is sufficiently small, we still recover a power law. For $\beta > 1$ we however find an exponential decay in $p(i)$. Given some $1/W < \beta < 1$ these priors can produce power laws with an exponential cut-off at $\beta i \approx 1$ (see figure 25).

Note that the prior probabilities constitute an absolute point of reference regarding which state is visited. We have not yet touched upon the question of relative transition probabilities. Those were kept fixed to be of the form in Eq. (4.2) such that there are equal probabilities to reach any point below the current state.
In the Oslo model, it turns out, we are dealing with a prior distribution that has regions of exponential increase and decrease.

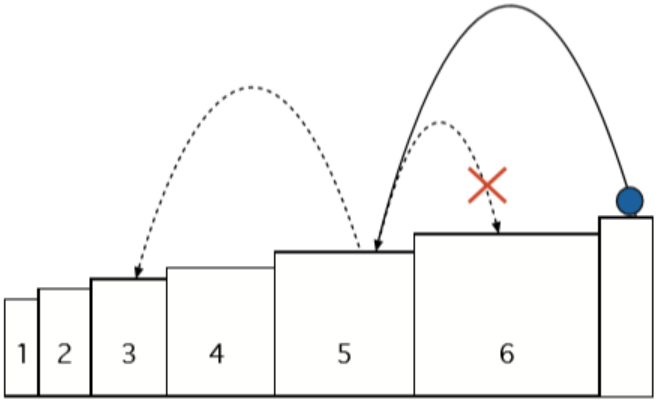

Figure 24: A ball falls down a staircase and can never jump back upwards, but will reach all steps below with a probability proportional to the area. Figure taken from [25].

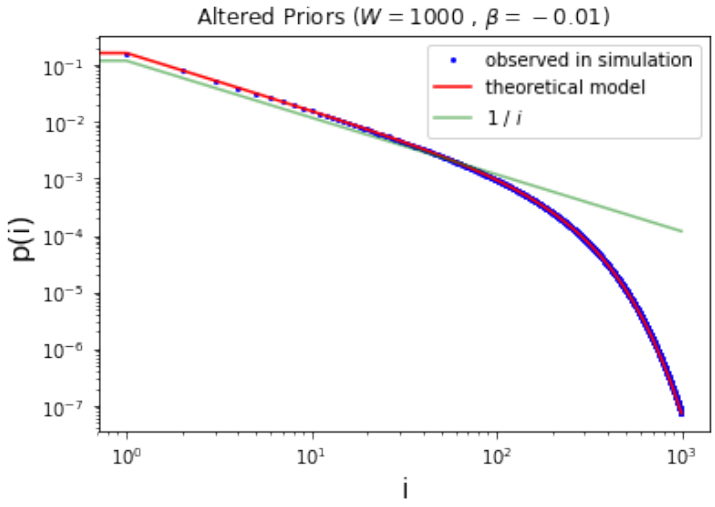

Figure 25: Results of a slowly driven SSR simulation using exponential priors $q(i) = \exp -0.01 \cdot i$. For large values of i, the found distribution decays exponentially (blue dots). This essentially happens as the states with $i > 100$ are dominated by the driver. For $i < 100$ we find Zipf's law as approximation (green). Equation (4.11) was compared with the simulation (red).

4.4 SSR processes with arbitrary driving probabilities

Corominas et al. have also studied the influence of the driving mechanism in [30] & [25]. By adding random noise to the system, that is a non-zero probability λ_n for every state i to jump to any other random state j. In this way two processes are mixed: the slowly driven SSRP and a form of undirected random walk. There is a probability that the process restarts at any point. [25] have shown that adding such a mechanism to the system, alters the exponent in the resulting power law attractor $p_{\lambda=1}$,

$$p_{\lambda=1}(i) = p(1) \cdot i^{1-\lambda} \qquad . \tag{4.12}$$

Consistently a uniform distribution is recovered for $\lambda = 1$, which is produced by the mere random walk.
In [30] the authors allowed λ to be state dependent. Interestingly $\lambda(i)$ can create a whole range of different attractor configurations for the distribution of state visits. Given a certain $\lambda(i)$ the resulting $p(i)$ can be even computed analytically, using an implicit relation, Eq. (4.13), which holds for large sample spaces where a continuous approximation $i \to x$ is applicable,

$$\lambda(x) = -x \cdot \frac{d}{dx} \log p_{\lambda=\lambda(x)}(x) \qquad . \tag{4.13}$$

Linearly increasing restart probabilities $\lambda \propto i$ will for instance produce exponential distributions.
We will later on measure $\lambda(i)$ for the Oslo model.

4.5 SSR processes with fixed driving intervals

Driving in the present form initially places the ball on the staircase at a random step. In case of a sandpile the driver is essentially the addition of a grain at position $x = 1$. This is a constant addition in terms of i representing energy, rather than a reset to a random configuration. Therefore I will discuss a SSRP where the ball is lifted a total of k steps whenever it is driven with probability λ. The priors, $q(i)$, are kept uniform. The transition probabilities in question are also visualized in figure 26 and can be expressed as

$$p(j \mid i) = \begin{cases} \frac{1-\lambda}{i-1} & i > j \\ \lambda & j = i + k \end{cases} \qquad . \tag{4.14}$$

If k is large and λ chosen to be small, then the process actually splits into N/k regions. As λ is small the process mostly collapses to the ground state. From there it may be driven to higher domains with an exponentially decaying probability, as each individual jump k has a probability λ. Within j steps a total jump of $j \cdot k$ can occur,

$$p(j \cdot k \mid 1) \approx \lambda^j \qquad .$$

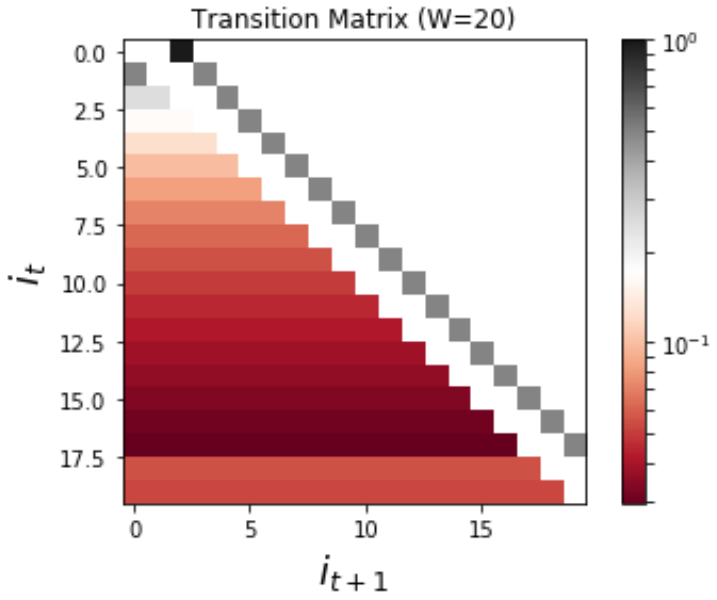

Figure 26: A color coded transition matrix to visualize the structure of Eq. (4.14). $k = 2$ and $\lambda = 0.5$ in this picture.

From that excited position the process is likely to then reach to a position with i being relatively small and it will be driven again. By that process the power law of the lowest region is replicated with exponential decay. Figure 27 shows the discussed behaviour.
If we tune λ to be large, we eventually encounter a regime in which the driving process and the relaxation process are balancing each other. Neither is the process saturated in the ground state, nor in the highest possible state. Such curves can be seen in figure 28 & 29.
States in the Oslo model are also subject to such a balance between driving and relaxation process. As it will be shown later, this leads to a somewhat Gaussian peak for the visiting distribution of many discussed macro variables in the Oslo model.

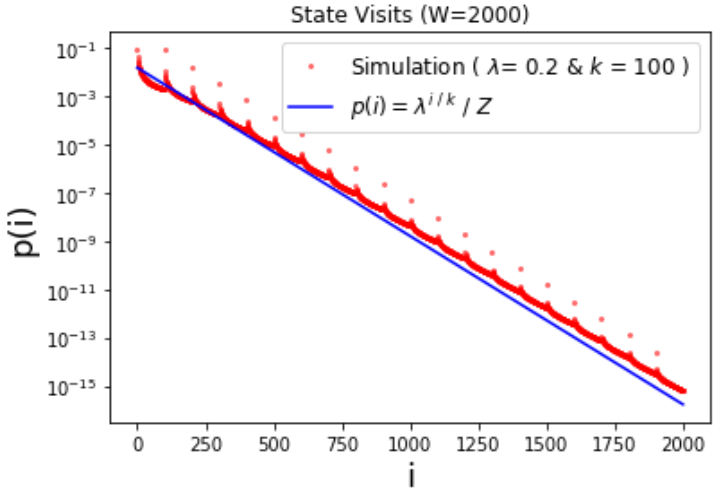

Figure 27: Attractor of a SSR process with a fixed driving interval of $k = 100$. $\lambda = 0.2$ is relatively small. The red line is globally exponentially decreasing, but features 20 distinct local domains, that feature a decrease on their own and form a sort of smooth saw-tooth like structure. Each local decay (each saw-tooth) decreases as a power law. This happens because any of those is essentially a copy of the lowest domain, which relaxes just as a slowly driven SSRP. The overall structure is decreasing as an exponential function $\approx \lambda^{i/k}$, as expected from the fact that $p(j \cdot k \mid 1) \approx \lambda^j$.

4.6 SSR processes with altered transition probabilities

Finally lets look at the transition probabilities. So far only the micro-canonical realization, Eq. (4.2), was discussed. A given dynamical system might however feature transition probabilities that depend on the relation of initial state i and final state j of a transition.

Given a initial state we could for instance consider a canonical or exponentially distributed choice of final states. This can be done in different ways. Either we fix an external heat bath with temperature T_0 and connect it to our system, or we let the temperature of the bath depend on the current sample space size ($T_\Omega = T(\Omega)$). The first option was already realized by implementing exponential prior probabilities with fixed β. To realize the other we allow $\beta = \beta(\Omega)$.
In general there can be many different realizations. I would like to constrain the analysis to such processes that feature scale free relaxation dynamics. That is, independent of the current size of the sample space, the structure of the transitions will remain the same. Mathematically we write

$$p\left(\xi \cdot j \mid \xi \cdot i\right) = \xi^{-1} \cdot p\left(j \mid i\right) \qquad . \tag{4.15}$$

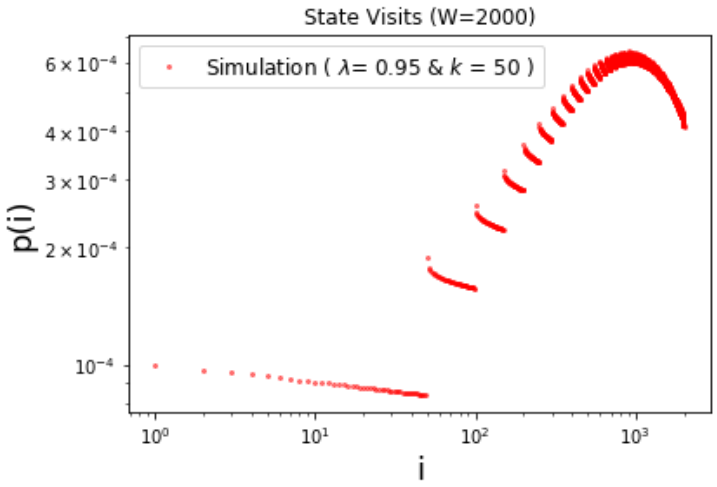

Figure 28: Same as figure 27 but with a different choice of parameters. Now λ is relatively large. Low states are less likely to be visited, as the driver pushes them up again. Thereby a peaked structure emerges at an intermediate state i as a result of the balance between driving and relaxation. Note that the plot features double logarithmic axes. The decrease of the first domain (lower left corner) is a power law with slope -1.

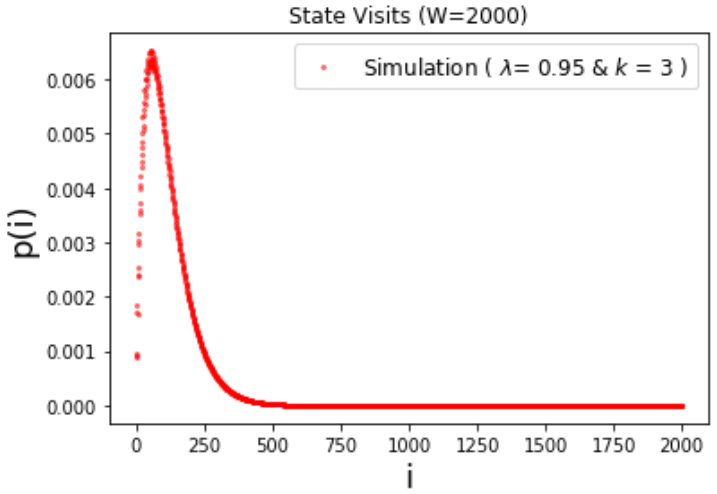

Figure 29: For small values of k the domain structure vanishes as domains contain only one or two states. The overall single moded behaviour remains.

If the sample space is expanded by a factor ξ, then the transition probability shall remain the same as in the unexpanded case, but be stretched and normalized.
The power law transition $p(j \mid i) \propto i^{-1}$ for instance suffices this constraint,

$$p\left(\xi \cdot j \mid \xi \cdot i\right) = \frac{1}{\xi i} = \xi^{-1} \cdot p\left(j \mid i\right) \qquad .$$

So does an exponentially decaying transition probability, where we set (as discussed above) $\beta^{-1}(i) \propto i$ or $T(i) \propto i$,

$$p(j \mid i) = \begin{cases} exp\left(\frac{-b\cdot(i-j)}{i}\right) \cdot Q^{-1}(i) & i > j \\ exp\left(\frac{-b\cdot(W-j)}{W}\right) \cdot Q^{-1}(W) & i = 1 \\ 0 & else \end{cases} \qquad . \tag{4.16}$$

Simulations show that, despite the exponential character of the transition probability, Zipf's law can be recovered also in this case. While $\beta = const.$ breaks the power law, as we have seen for the case of exponential priors, a scale free formulation of transition probabilities was enough to restore its emergence. Figure 30 shows the convergence to a power law of power -1 for three different orders of our parameter b.

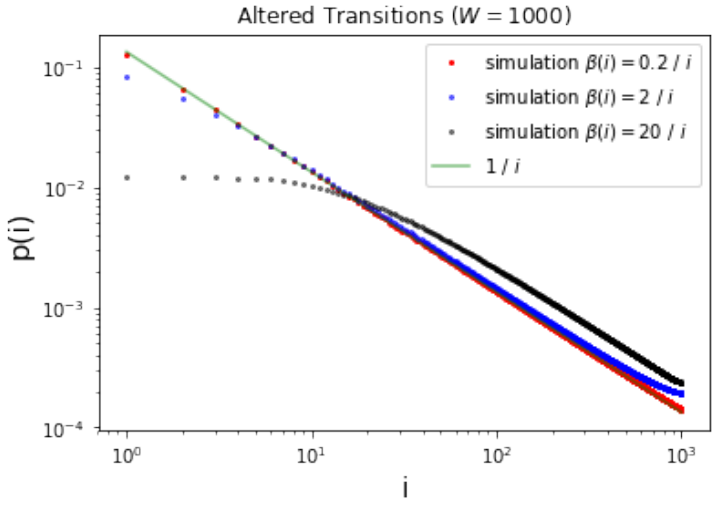

Figure 30: A slowly driven SSR with transitions of the form in Eq.(4.16) was studied. Shown are three different runs with values of $b \in \{0.2, 2, 20\}$ and $\beta(i) = b/i$. Despite some initial deviations, all runs converged to Zipf's law.

While we can speculate on the universality of Zipf's law for transition probabilities of the form in Eq. (4.2) or Eq. (4.16), Markov chains, that do not satisfy the scale free structure given in Eq. (4.15), do not necessarily give rise to a

power law. A quick counterexample would be a process where at each step the sample space size is only reduced by 1. Such a process would reach any state with equal probability on the course of a relaxation.
The Oslo model has a special relaxation probability that, as I will argue in the next chapter, stems from a branching process. A single avalanche can initiate further avalanches on the way.

4.7 Avalanches in SSR processes

Next, I want to make a short comment on the avalanche statistics of SSRPs. Let us define an avalanche as a downward transition between i and j, with $i > j$. The corresponding size of an avalanche equals $s = i - j$. What are the statistics of this quantity? Given that we already know $p(i)$, the visiting distribution of state i, $\hat{p}(s)$, the probability of an avalanche with size s to occur, can be computed by summation,

$$\hat{p}(s) = \sum_{i=s}^{W} p(i-s \mid i) \cdot p(i) \qquad . \tag{4.17}$$

For the slowly driven SSR process with transition probabilities given in Eq. (4.2) for instance, we readily conclude that also the distribution of s follows Zipf's law,

$$\hat{p}(s) = \sum_{i=s}^{W} \frac{p(1)}{i^2} \approx \int_s^W \frac{p(1)}{i^2} di = p(1) \cdot \left(\frac{1}{s} - \frac{1}{W} \right) \propto \frac{1}{s} \qquad .$$

An interesting quantity in the Oslo model is the avalanche size: What is the size of a transition from one state of load κ_i to reach another load κ_j. The corresponding avalanche size is then nothing else than $s = \kappa_j - \kappa_i$. With the statistics of κ it will be possible to derive the avalanche statistics using Eq. (4.17).

4.8 Universality of the result

At the beginning of this section we have commented on the derivation of Eq. (4.1) - the canonical ensemble - and seen that it can be deduced by maximizing Shannon's entropy. Hanel et al. [31] have shown that it is in fact possible to perform a similar analysis for the case of a SSR process (acting very much in the spirit of E.T. Janes). However, as we are dealing with a system, which is per se non-ergodic and has a broken detailed balance, the simple form of Shannon's entropy does not apply anymore. Rather a new entropy functional had to be found first (see also [32]). For the case of the slowly driven SSRP one finds

$$S_{SSR} = -\sum_{i=2}^{W} \left[p(i) \log \left(\frac{p(i)}{p(1)} \right) + (p(1) - p(i)) \log \left(1 - \frac{p(i)}{p(1)} \right) \right] \tag{4.18}$$

In [31] this entropy, which entangles the different states of the system in an interesting way, is deduced and one finds Zipf's law as the distribution which maximizes S_{SSR}.

Remark on maximum caliber and SSR processes

I also tried to identify variables in the slowly driven SSR process which live in an ergodic space, that is not contracting or expanding. For instance, the states i are following SSR dynamics, but the phase space corresponding to the lengths of a relaxations process, τ, remains unconstrained as after each full collapse the sample space is reset. A more general way to put that idea is by considering a directed network on the space of states, which is decomposed into a fully connected undirected network on the space of circular paths as entities (see figure 31). Such an approach would allow an analysis using simple Shannon entropy for the computation of the maximum entropy configuration.

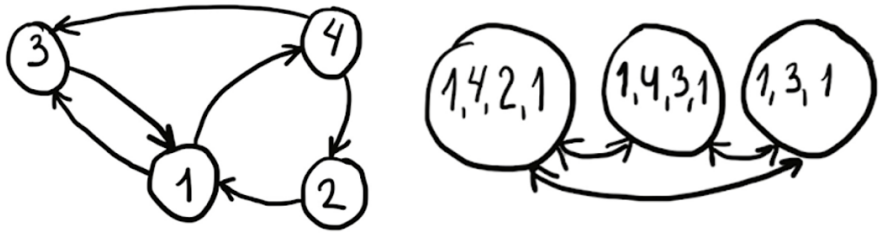

Figure 31: Left: A directed graph. Right: Its decomposition into full cycles. While the left graph has a diameter greater than 1, the right graph provides a representation of the same network, where all nodes are directly linked with each other.

But it is unclear which measure on the cycles should be statistically constrained in order to reproduce the observed power law. I tried the length τ or the sum of states visited during a relaxation process, but none of these seemed to be a good choice. I realized that the power law is a property independent of the cycle length τ. It appears even if we only look at those relaxations for which the relaxation times matched ($\tau = \text{const.}$) (figure 32),

$$p(i \mid \tau) \propto i^{-1} \qquad . \tag{4.19}$$

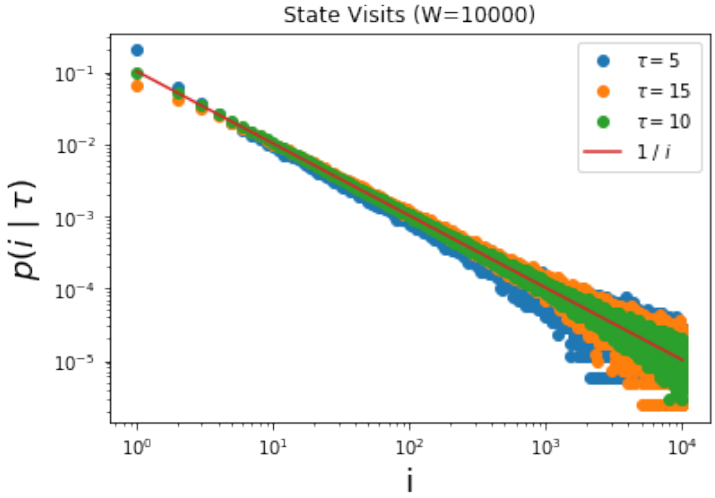

Figure 32: The statistics of state visits conditioned on different relaxation times ,τ, (points in different colors) still produce Zipf's law (red). Note that the variance of the green points ($\tau = 10$) has least variance. This is because runs with a relaxation time of $\tau = 10$ are more likely, as it can be seen in figure 23 for a slowly driven SSRP of same maximum sample space size W.

4.9 The choice of SSR variable

The variable of most interest in the OSM is undoubtedly the avalanche size s. It is measured as the amount of topplings happening throughout a relaxation and shows a distinct power law featuring a power of roughly -1.53 and a bump with exponential cut-off in the tail. It is hypothesized in [19] that this bump is triggered by relaxation events that drop sand out of the system.
The avalanches themselves are however not strictly reducing. We might observe a small avalanche, then drive the system, and measure a very large avalanche in the next relaxation event. Thus s directly is not sample space reducing. As we have however seen in chapter 4.7, scale-free avalanche statistics can still directly result from the sample space reducing property of an underlying variable i, such that $s_t = i_t - i_{t+1}$. In order to find appropriate candidates for the state variables i, we will have to consult some physical arguments.

Energy, mass and load

A natural choice of SSR variable clearly is the energy E. During a relaxation event, the potential energy can only be reduced. The resulting energy-difference ΔE will be dissipated in form of heat. Energy conservation thus sufficiently restricts the dynamics of E to reduce the sample space of reachable energy

states,

$$E(t) = E(t+1) + \Delta E \qquad . \tag{4.20}$$

The mass too, could be a reasonable choice of SSR variable. During a relaxation step the mass however does not necessarily have to decrease. If there is no outflow of mass observed, the total mass will remain equal. The mass as SSR variable is blind regarding internal reconfigurations of the rice pile.
Finally, the load κ was defined in such way that n toppling events directly correspond to a $\Delta\kappa = n$. In order to compare the observed power law statistics with the data in the literature regarding s, the load will be our best choice of SSR variable.
In order to capture the avalanche statistics of any of those variables, it will be necessary to perform our measurements on the set of stable or driven states $(\mathcal{S} \cup \mathcal{D})$.

Slope

Lets recall Eq. (3.9) for the mean slope acquired by a linear fit,

$$\alpha = 6 \cdot \frac{2\kappa - (L+1)M}{L(L^2-1)} \qquad .$$

First we notice that the slope is proportional to the load subtracted by mass, which we identified both to be sample space reducing. A relaxation event, that does not change the mass of the sandpile, is therefore SSR. On the other hand a relaxation event that ultimately triggers a grain at the boundary to leave the system, can rarely increase the slope defined in this way.
The pinned slope $\tilde{\alpha}$ defined in Eq. (3.10) is only tied to the dynamics of κ and therefore SSR. By studying κ we implicitly study the mean slope of the system.

Connection to the study of interfaces

One can also try to conjecture SSR variables by connecting the Oslo model with growing surfaces (as studied in [22], [33],[34]). [33] introduce the amount of topplings $T(x,t)$ a site has experienced throughout the existence of the pile and the amount of grains $G(x,t)$ that have been loaded onto the site x throughout the existence of the pile. Identifying $H(x) = T(x-1) - T(x)$ & the local stability $\eta(x,T)$ as a random noise, being either 1 or 2 in the space of (x,T), the authors make the following assignment:

$$F(x,t) = k(x,t) - \eta(x,T) \qquad . \tag{4.21}$$

F gives a type of "toppling force" acting on x. If $F > 0$ the site is going to

topple, else remains stable. Further,

$$\begin{aligned} F(x,t) &= H(x,t) - H(x+1,t) - \eta(x,T) \quad , \\ F(x,t) &= (T(x-1,t) - T(x,t)) - (T(x,t) - T(x+1,t)) - \eta(x,T) \quad , \\ F(x,t) &\approx \Delta x^2 \nabla^2 T(x,t) - \eta(x,T) \quad . \end{aligned}$$

The ∇^2-operator was deduced from the discrete Laplacian as a continuum approximation,

$$\nabla_x^2 T(x,t) \approx \frac{1}{\Delta x^2} \left(T(x-1) - 2T(x) + T(x+1) \right) \quad .$$

$F = 1$ means that the site x is going to topple once. Therefore, $T(t+1,x) - T(t,x) = F(t,x)$. However, if $F \leq 0$, nothing is going to happen,

$$\partial_t T(x,t) \approx \Theta_{[0,\infty]} \left(\frac{\Delta x^2}{\Delta t} \partial_x^2 T(x,t) - \eta(x,T) \right) \quad .$$

Despite the highly nonlinear Heaviside function, this equation has similarity with the so called Quenched Edward Wilkinson equation (qEW). [22] report that they even find the exact qEW equation for the dynamic variable $G(x,t)$,

$$\partial_t G(x,t) = \nu \partial_x^2 G(x,t) + \hat{\eta}(x,G) \quad . \tag{4.22}$$

Where $G(x)$ was identified to suffice

$$T(x,t+1) = \frac{1}{2} \left(G(x,t) + \hat{\eta}(x,G) \right) \quad . \tag{4.23}$$

Here $\hat{\eta}$ is 0, if G is even, & either 1 or -1 (with probability p and q), if G is odd. This equation describes the growth of a surface with height profile G, which is subject to a random addition of particles at different positions due to $\hat{\eta}$. However irregularities on the surface tend to diffuse as well. The "surface" growing here is the abstract height of $G(x,t)$. The boundary conditions in the continuum description are $\partial_t G(L,t) = 0$ and a constant velocity field pulling the origin $\partial_t G(0,t) = v$ through external driving.
We can try to reinterpret the term $\partial_x^2 G(x,t)$ as resulting from a gradient flow acting on the potential $W(t)[G]$,

$$\partial_t G(x,t) = -\nu \frac{\delta W[G]}{\delta G} + \hat{\eta}(x,G) \quad . \tag{4.24}$$

$W(t)[G]$ of the following form,

$$W(t)[G] = \frac{1}{2} \int_0^L K(\partial_x G) dx = \frac{1}{2} \int_0^L (\partial_x G(x,t))^2 dx \quad , \tag{4.25}$$

will suffice. We can proof this claim by invoking some variational analysis.

$$\frac{\delta W[G]}{\delta G} = \frac{\partial K}{\partial G} - \partial_x \left(\frac{\partial K}{\partial (\partial_x G)} \right) = -\partial_x^2 G \tag{4.26}$$

The process therefore describes G as evolving towards minimizing W. W receives an abstract interpretation, since it can be identified with $\phi(G)$, the total arc length of the curve, spanned by G, since

$$\phi(G) = \int_0^L \sqrt{1 + (\partial_x G)^2} dx \approx W_0 + W \qquad . \tag{4.27}$$

A minimization of W therefore equals a minimization of $\phi(G)$. In other words: During a relaxation process, the surface length, as spanned by G will decrease. But also a more physical interpretation can be found: $G(L+1)$ is the amount of grains that dropped out of the system. $G(L)$ is equal to that amount, plus all grains that reside on site $x = L$: $G(L) = H(L) + G(L+1)$. A continuation of this scheme allows the identification of $G(x)$ with the mass of a sandpile with size $L = x$, since

$$G(x) = \sum_{y=x}^{L} H(y) + G(L+1) \propto M_{L=x} \qquad . \tag{4.28}$$

Therefore the surface spanned by $G(x)$ is actually proportional to the potential energy of the system,

$$W = \frac{1}{2} \int_0^L (\partial_x G(x,t))^2 dx = \int_0^L \frac{H(x)^2}{2} dx = E \qquad .$$

Also in the continuous case we very naturally find the result that the energy E of the system is a SSR variable that controls the dynamics of the system.

Surface length

The preceding analysis motivates us to look at surface lengths as potential SSR variables. We will do this by tracing the surface length φ. To see that the surface length is almost SSR, but not quite, we first note that if the quantity

$$\sum_x k(x)^2 = \varphi_2$$

is strictly reduced during a relaxation, then also φ. This is easily justified using the triangle inequality,

$$\left(\sum_x \sqrt{k(x)^2 + 1} \right)^2 \leq \sum_x k(x)^2 + L \qquad .$$

A toppling event at a position y that is not at the boundary will take place only if $k(y) \geq 2$. The toppling site looses two slope elements $k(y) \to k(y) - 2$ while its neighbours gain one each. While the rest of the sum remains unchanged, we

therefore have after a toppling,

$$\varphi_2(t+1) = \sum_{x=1}^{y-2} k(x,t)^2 + (k(y-1,t)+1)^2 + (k(y,t)-2)^2 + (k(y+1,t)+1)^2 + \sum_{x=y+2}^{L} k(x,t)^2 \quad .$$

At the boundary the expression has to be changed accordingly. For the differences $\Delta\varphi_2(t) = \varphi_2(t+1) - \varphi_2(t)$ we find depending on the toppling site y,

$$\Delta\varphi_2(y(t),t) = \begin{cases} 5 + 2k(y+1,t) - 4k(y,t) & , y = 1 \\ 6 + 2k(y+1,t) + 2k(y-1,t) - 4k(y,t) & , L > y > 1 \\ 2 + 2k(y-1,t) - 2k(y,t) & , y = L \end{cases} \quad . \tag{4.29}$$

φ_2 is SSR, only if

$$\varphi_2(t_s) \geq \varphi_2(t_e) \quad , \tag{4.30}$$

$$0 \geq \sum_{t=t_s}^{t_e} \Delta\varphi_2(t) \quad .$$

Here t_s is the start of a toppling cascade, t_e the time of its end. As any cascade has to start at site $y_{t_s} = 1$, the boundary, we have

$$\Delta\varphi_2(1,t_s) = 5 + 2k(2,t_s) - 4k(1,t_s) \quad .$$

The cascade can halt immediately at $t_s + 1$ if $k(2,t_s) \leq 1$. Then, as $k(1,t_s) \geq 2$, the condition, given by Eq. (4.30), is met. If $k(2,t_s) = 2$, the cascade will go on with certainty and the surface is increasing intermediately:

$$\max(\Delta\varphi_2(t_s)) = +1$$

A cascade at position $y_{t_s+1} = 2$ will be induced. Let us first assume that the cascade only travels downwards and passes position y_t. First $k(y_t)$ will increase by 1 at $t-1$, then decrease by 2 at t, then increase again by 1 at $t+1$. After the passage of the cascade $k(y_t)$ remains unchanged. This is similar to a mouse moving under a blanket: The mouse will always create a little mount in the surface of the blanket. But the mount will move with the mouse, such that the surface of the blanket remains unchanged. If the cascade halts at position y_{t_e} the total change in φ_2 only depends on the slope values at the start and the end of the cascade.

$$\varphi_2(t_e) - \varphi_2(t_s) = 3 - 2k(1,t_s) - 2k(y_{t_e} - 1, t_s) + 2k(y_{t_e}, t_s) \tag{4.31}$$

As we require that site 1 is ≥ 2 and $y_{t_e} - 1$ is ≥ 1 in order to be able to topple and $y_{t_e} \leq 1$ for it to become stable, the total change is negative,

$$\max(\varphi_2(t_e) - \varphi_2(t_s)) = -1 \qquad .$$

If the avalanche hits the boundary at $t_e - t_s = L$ and stops, we find

$$\varphi_2(t_e) - \varphi_2(t_s) = 3 - 2k(1, t_s) - 2k(L, t_s) \qquad . \tag{4.32}$$

In this case $\max(\varphi_2(t_e) - \varphi_2(t_s)) = -3$. The loss of surface is even stronger. The mouse has left the blanket.

Due to the Abelian property we can first follow a single cascade downwards and afterwards discuss any further cascades it may induced at time t_i. In a similar logic as before, any relaxation event induced at $y_{t_i} = y$ and ending at $y_{t_e} = y'$ will create a change in slope proportional to

$$\varphi_2(t_e) - \varphi_2(t_i) = 4 - 2k(y, t_i) - 2k(y', t_i) + 2k(y - 1, t_i) + 2k(y' + 1, t_i) \qquad . \tag{4.33}$$

If we want that the pile becomes stable at t_e, the maximum of this difference $\max(\varphi_2(t_e) - \varphi_2(t_i)) = 2$. This maximum is only reached in the rare case that $k(y-1, t_i)$, $k(y'+1, t_i)$ and $k(y', t_i)$ are equal to 1.
Adding up the changes in slope we find that the surface can indeed grow for a relaxation event. However it is quite unlikely, as this only occurs for very peculiar circumstances. Most transitions will either reduce the surface length or keep it approximately equal. Further, this analysis shows that the largest reductions in surface length occur if sites at the boundary are involved.

Height $H(1)$ and n_2

We can rewrite φ_2 as $\varphi_2 = 2n_1 + 4n_2 + 9n_3$. n_j is the number of times a slope of size j is observed in the configuration of the pile. We then compare this expression with the height $H(1)$,

$$H(1) = n_1 + 2n_2 + 3n_3 \qquad . \tag{4.34}$$

$H(1)$ is proportional to the mean of $k(x)$, while the surface length is proportional to its second moment. For any stable configuration we can remove the slopes of 3 from the equations and rewrite

$$H(1) = L + n_2 - n_0 \qquad , \tag{4.35}$$

$$\varphi_2 = L + 3n_2 - n_0 \qquad . \tag{4.36}$$

If we also take into account the fact, that any $k = 0$ is generally counterbalanced by a $k = 2$, we can conclude that both quantities are quite sensitive to n_2. n_2 itself is not a SSR variable, for similar reasons why the surface length is not. $H(1)$ is SSR.

5 The Oslo Model As SSR Process

Now, after having discussed the necessary basics, we wish to continue to present the main results of my work. In chapter 4 we have presented the necessary toolset to analyse SSRPs and discussed which variables can be expected to have SSR dynamics. We will try to capture the statistics of avalanches in the Oslo model by studying the SSR behaviour of the discussed state variables of interest.

5.1 Observed distributions

Visiting distributions

Here I present the observed visiting distributions in $\mathcal{S} \cup \mathcal{D}$ for the set of (almost) SSR variables discussed above (figure 33) and the non SSR variables n_0 & n_1 (figure 34). All plots in figure 33 and 34 show Gaussian shapes, $\propto \exp\left(-k_1(x-x_0)^2\right)$, at first glance. Logarithmic vertical axis however show that the tail towards the higher values decays significantly slower, more like $\propto \exp\left(-k_2 x\right)$. The effect is especially strong for M, κ and E. In order to quantify differences among visiting distributions we calculated average, μ, standard deviation, σ, skewness, γ, and Person kurtosis, ω, of the histograms of different measures (here exemplarily for $L = 100$) in table 1.
Measures with relatively larger kurtosis, like mass, energy and load, are associated with a larger fraction of events in the tails. The surface length and height, on the other hand, obey shapes that resemble skewed Gaussians, as their kurtosis is relatively low. This difference will become even more evident as we start looking at avalanche distributions. All measures, despite n_1, are asymmetric, with the majority of events to the left of the maximum. n_0, in particular, is almost resembling an exponentially decaying distribution.

	μ	σ	γ	ω
M	8766	83	0.438	0.298
E	511018	9194	0.473	0.352
κ	585468	5275	0.444	0.303
φ	199	1.50	0.231	0.071
$H(1)$	171	1.82	0.236	0.094
n_2	72.6	1.91	0.194	0.020
n_1	25.7	2.59	-0.281	-0.001
n_0	1.55	1.14	0.590	0.173

Table 1: Mean μ, standard deviation σ, skewness γ and kurtosis ω of visiting distributions computed with *Numpy* [35].

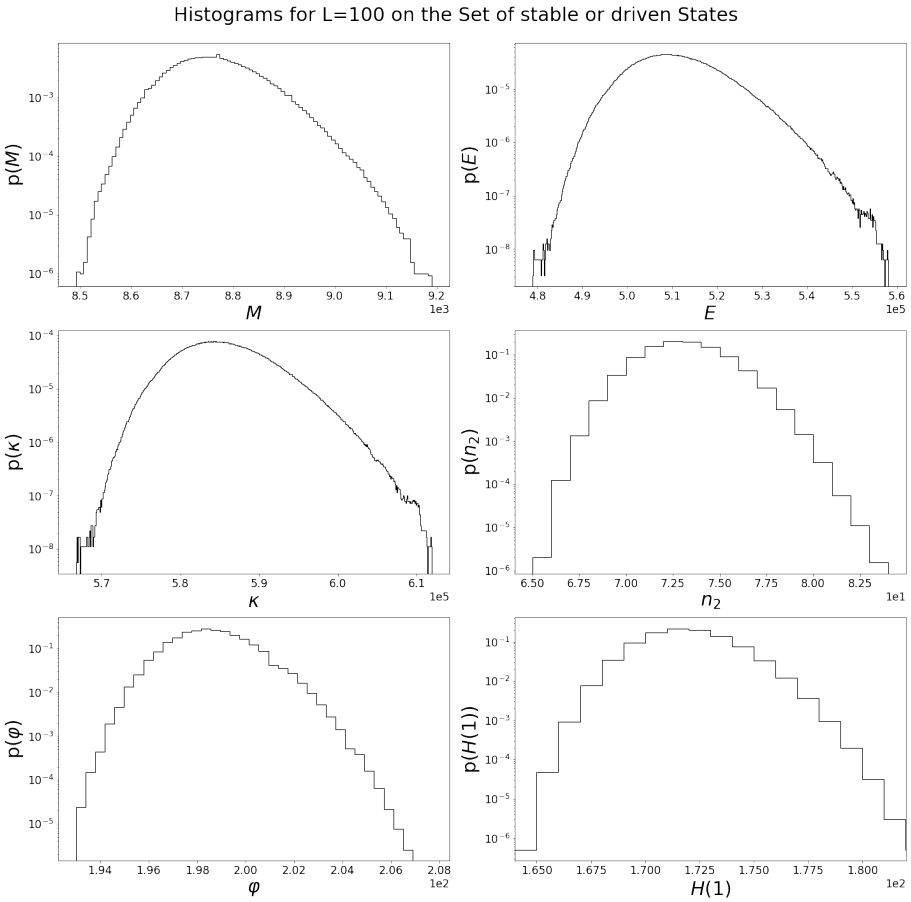

Figure 33: A selection of visiting distributions observed in the simulations. In order of reading: Mass M, energy E, load κ, slopes of 2 n_2, surface length φ and height $H(1)$.

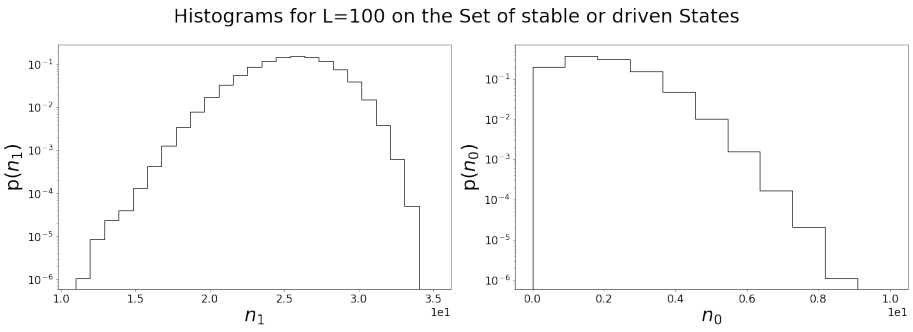

Figure 34: Visiting distributions of n_0 and n_1.

Avalanche distributions

The avalanche dynamics show diverse behaviour. We will order the macro measures according to the patterns emerging in their avalanche distribution.

- *Powers of* -1.53 *with exponential cut-off (bump)*: Load κ, energy E, average slope α
  See figure 35. Load, energy and average slope have avalanche distributions that are decaying like a power law with an exponential cut-off. The cut-off is associated with a "bump": A local maximum, before the exponential decay sets on.

- *Poisson like dacay or bump*: Mass M
  See figure 36. The size of mass loss events has exponentially decaying probability for larger avalanches. For small avalanches the loss is increasing until it reaches a local maximum.

- *Exponential decay*: Height $H(1)$, slope two number n_2, surface length φ
  See figure 37. Height-, n_2- and surface length- changes are distributed according to an exponential decay.

Let us discuss why it is very natural that there exist these 3 distinct modes of avalanche size distributions. We may see an avalanche as a stochastic propagation of instabilities. The instability can travel in both directions, up-hill and down-hill, and even trigger further instabilities, topplings, on the way. The size of the full tree of stochastic trajectories performed by the instabilities is associated with changes in E or κ. Any trajectory that hits the boundary at $x = 1$ will reduce $H(1)$ by one, while any trajectory hitting the other boundary at $x = L$, will reduce M by one.

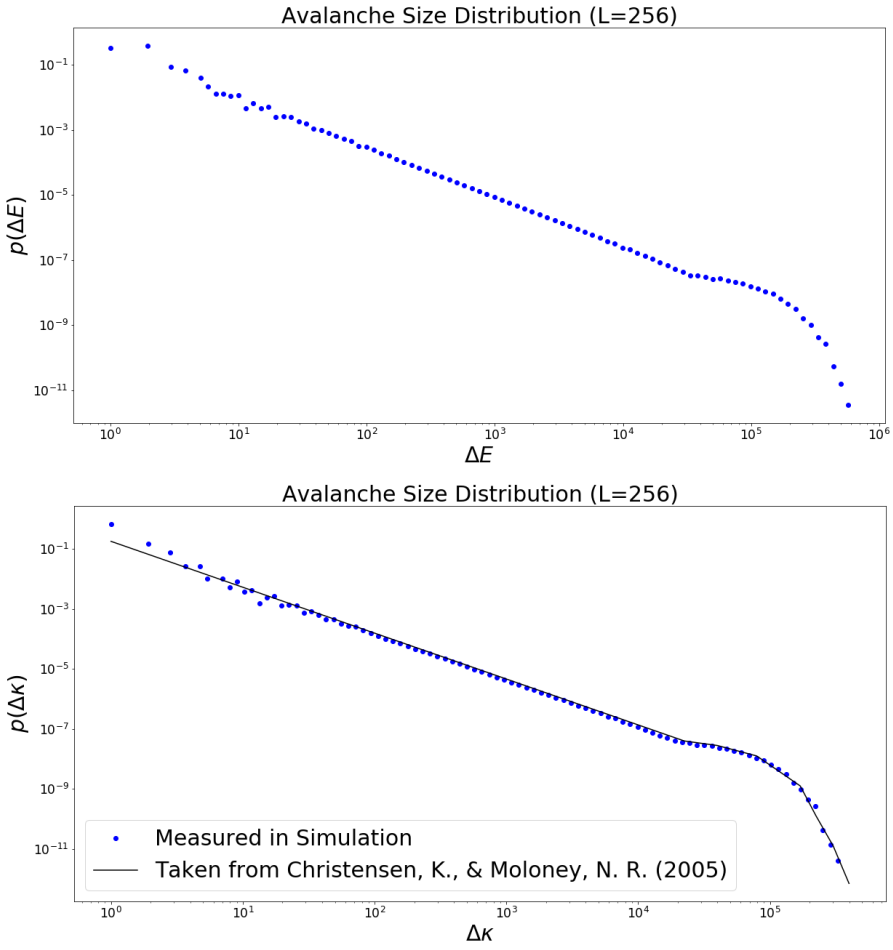

Figure 35: Energy E and load κ follow very similar dynamics. Deviations are mainly concerned with small transitions. The avalanche distribution decays like a power law with cut-off. The cut-off features a local maximum, the bump. My measurements of κ-avalanches are compared with the function found in the literature for the size of toppling events [19]. Curves match closely.

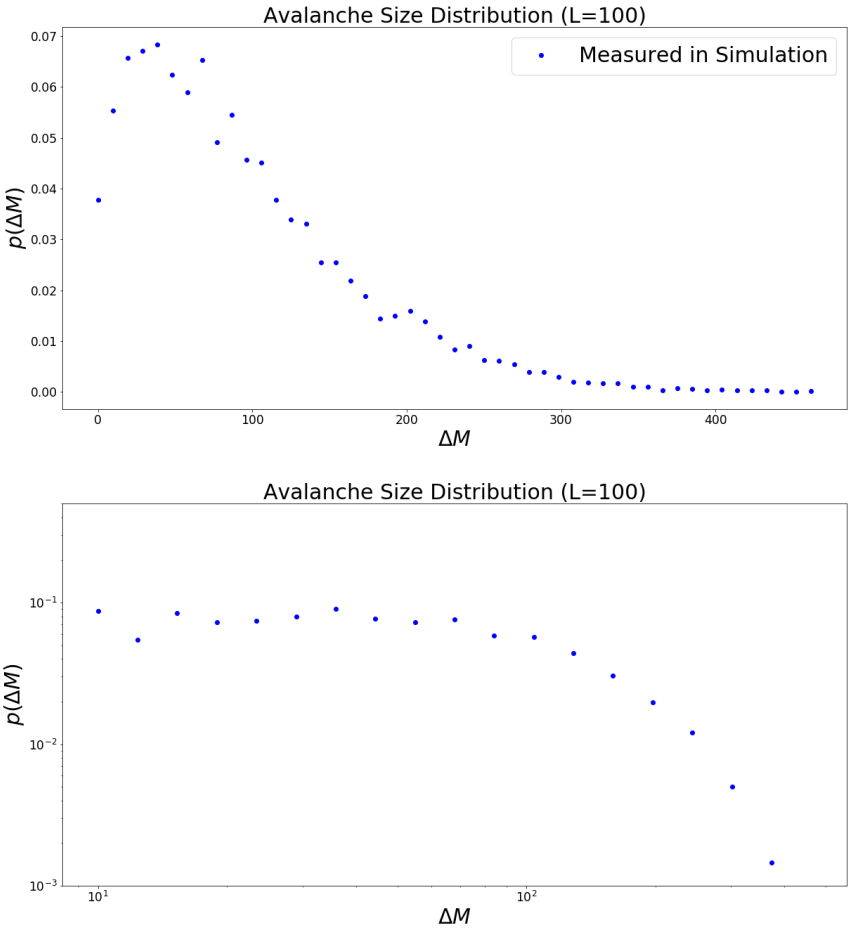

Figure 36: The mass M features a maximum in avalanche size, which quickly decays towards larger avalanche sizes. Plotting in a double-logarithmic way,one finds the same shape as the exponential bump observed in figure 35 for the energies. One concludes that the bump is associated with avalanches that reach the boundary at $x = L$.

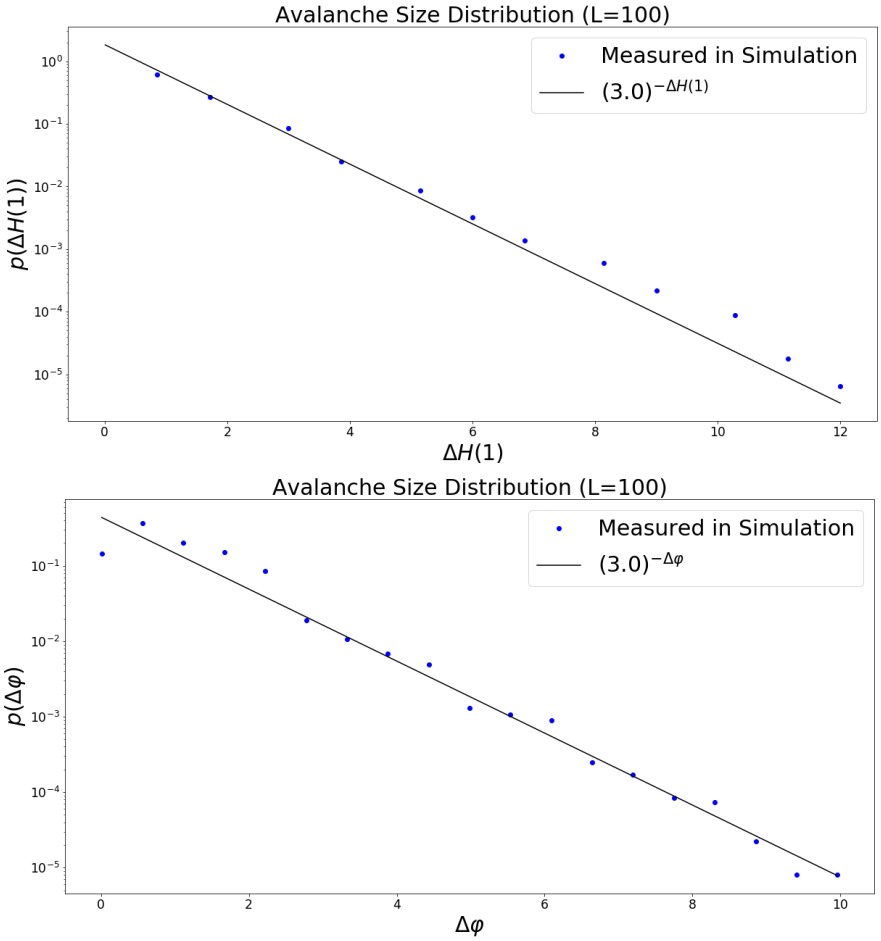

Figure 37: The peak height $H(1)$ and the surface length φ are decaying exponentially. The black lines quantify the strength of decay. The probability of a drop in height or surface length is cut to a third with each additional reduction of $\Delta H(1) = -1$, or $\Delta\varphi = -1$.

5.2 Driving events

A main ingredient to any SSR model are driving events. Most macro variables behave in a way such that a driving event increases them by a certain quantity d (see section 4.5). In the case of energy, d_E equals the current height of the pile $H(1) + 1$, as a new grain dropped onto the peak will carry that potential energy. d_M and d_κ on the other hand are constant 1 or L respectively.
A driving event may be initiated with a rate $\lambda(i)$ that depends on the state i. Note that on the set of stable and driven states, which is of main interest in order to reproduce the avalanche dynamics with a SSR methodology, relaxation events and driving events take turns ("tick-tock"). Each driving event $i \to j$ is immediately followed by a relaxation $j \to j - \Delta$, where $\Delta \geq 0$. The average driving rate $\langle\lambda\rangle$ therefore has to approximately equal 0.5. One might note that any state with a flat top (meaning $k(1) = 0$) is driven twice in a row. By counting $\Delta = 0$ as a relaxation we can however formally restore the tick-tock behaviour. We performed the analysis with both methods, using $\Delta \geq 0$ and $\Delta > 0$. We can write

$$\langle\lambda\rangle = \sum_i \lambda(i)/W = \frac{1}{2} \quad , \tag{5.1}$$

where W is the total number of accessible states. If the relation does not hold, this can only indicate that the chosen macro variable is in fact not SSR. This is because any SSR variable has to be increased during a driving event. If it were decreased during a driving event, as it for instance rarely occurs for the surface length, the tick-tock character is lost.
The tick-tock behaviour can still establish longer periods of growth, as long as relaxation processes remain minor. Typically a longer growth phase is stopped by a larger avalanche. This can be seen in figure 38, where not only the dynamics of single macro measures are shown, but also the average λ was calculated for various measures.
In order to arrive with the state dependent rate $\lambda(i)$, I proceeded in the following way: For any load state κ_i for instance, the number of visits n are counted on two different sets: The set of stable states $\mathcal{S}$ and the set of driven and stable states $\mathcal{D} \cup \mathcal{S}$. If a state is rather stable $n_{i,s} > n_{i,d}$, this indicates that the state has a higher than 1/2 rate of driving. This is because any stable state has to be driven in the next step. If, on the other hand, a state i is driven more frequently, its $\lambda(i) < 1/2$, as any driven state will be relaxed in the next step. In this way we identify $\lambda(i)$, given the stable visits $n_{i,s}$ and stable & driven visits $n_{i,d+s}$ for sufficient amounts of data,

$$\lambda(i) = \frac{p(i, i \in \mathcal{S})}{p(i, i \in \mathcal{S} \cup \mathcal{D})} \approx \frac{n_{i,s}}{n_{i,d+s}} \quad . \tag{5.2}$$

Measurements of this quantity can be seen in figure 39.

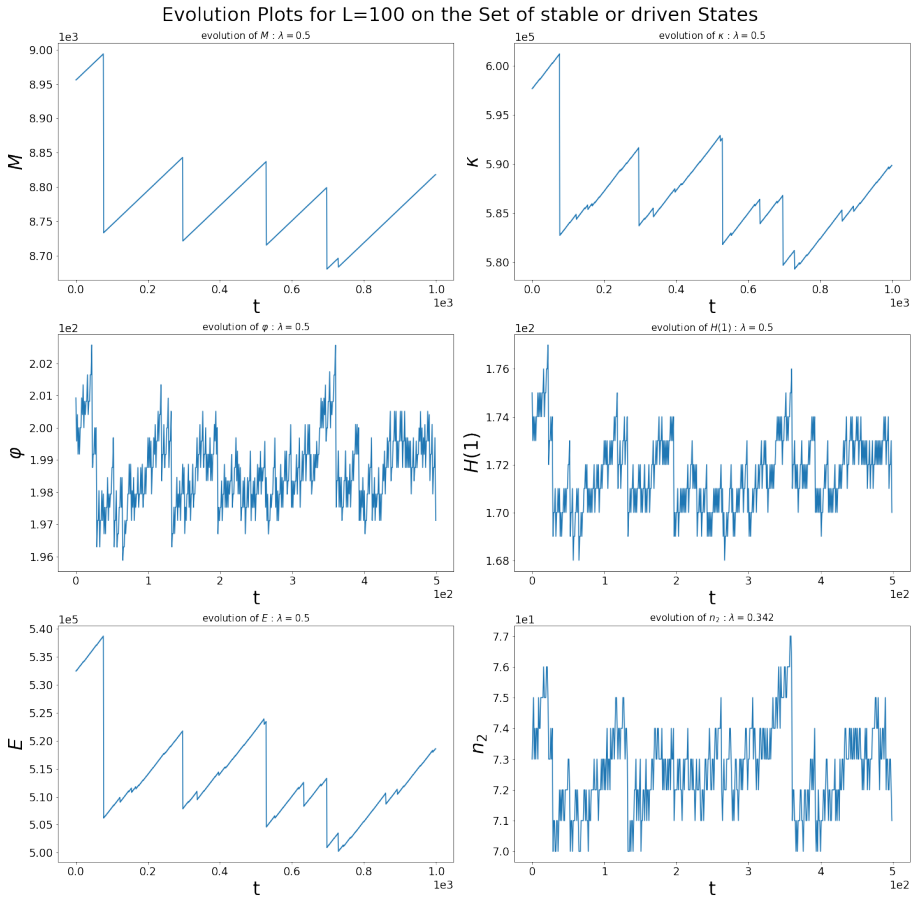

Figure 38: Dynamical variations of macro measures in the long term limit (non-equilibrium steady state): For load, energy and mass, growth phases can last for long periods and are abruptly stopped by an avalanche. Surface length, height and n_2 on the other hand rise and fall on a smaller timescale. Also average values of λ were calculated. While most measures, including the surface length, have an average driving rate of 0.500 (up to 3 digits), a considerable fraction of relaxation processes drive n_2.

For the sake of completeness I show how one would proceed in order to study the situation for non-zero relaxation events with $\Delta > 0$. All states that became unstable and which induced a non-zero relaxation, can be counted as $n_{i,r}$. Then, if we call this altered definition for the driving rate $\tilde{\lambda}(i)$, one finds

$$\tilde{\lambda}(i) \approx 1 - \frac{n_{i,r}}{n_{i,d+s}} \quad . \tag{5.3}$$

Using this definition Eq. (5.1) does not hold any more. In fact, take for instance the situation of mass: A relaxation only occurs in the relatively rare case of a mass excess. The measure will be driven more frequently than relaxed,

$$\langle\tilde{\lambda}\rangle \geq \frac{1}{2} \quad . \tag{5.4}$$

Two qualitatively different behaviours are observed:

- Load, energy and mass roughly have constant $\lambda(i) = 0.5$, with a very slight decrease towards higher states. Only for the highest states the driving rate quickly decays, and the lowest states conversely are driven with great certainty. With i_{min} and i_{max} being thresholds, we can write by means of simplification

$$\lambda(i) = \begin{cases} 1 & i < i_{min} \\ 0 & i > i_{max} \\ 0.5 & else \end{cases} \quad . \tag{5.5}$$

- Height and Surface Length appear to roughly follow a linearly decreasing $\lambda(i)$. Say,

$$\lambda(i) = \frac{W - i}{W} \quad . \tag{5.6}$$

Note that the driving rate will very well depend on the history of a given trajectory that reached that state. A trajectory that just reached state i by a relaxation from above will actually be driven with certainty, due to the "tick-tock" dynamics. We will later show that breaking this conditionality, and setting a simplified driving rate to be state-dependent only, does not alter the observed distributions. A state that just relaxed, will be allowed to relax again in this picture.

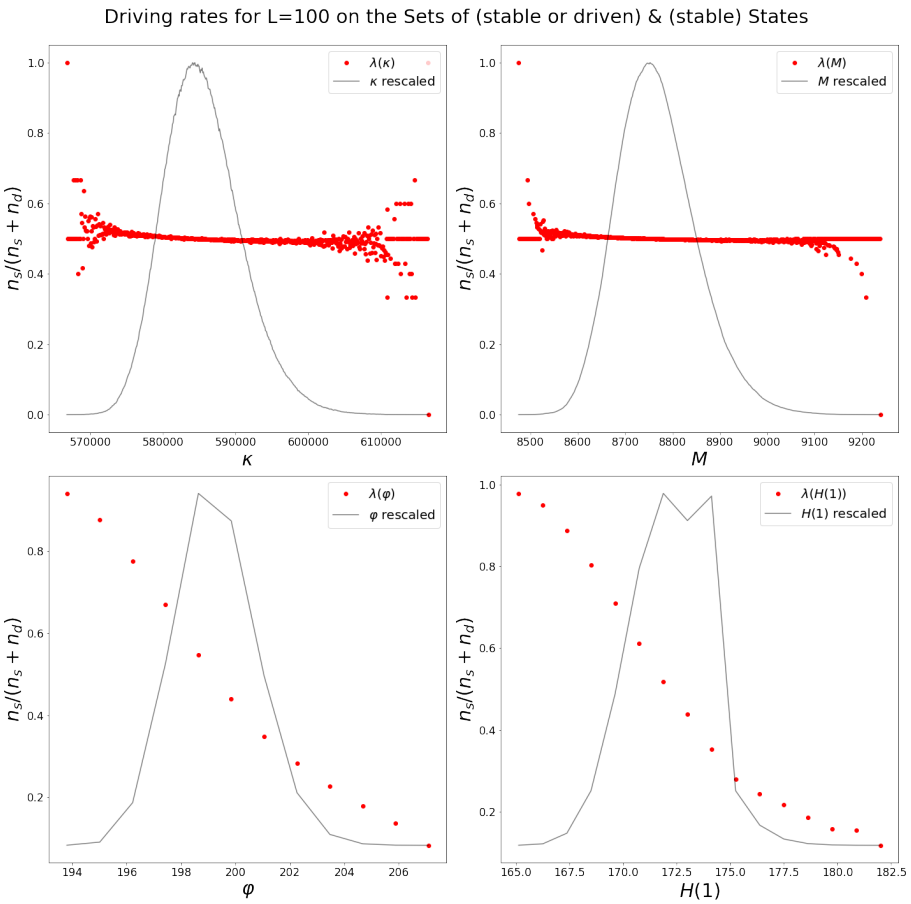

Figure 39: Red points: Driving rates as calculated with Eq. (5.3). As data points become scarce for extreme loads and masses, the variance increases on the sides. Black line: Rescaled visiting distribution in the set of stable and driven states. These are shown in order to put the relation of driving rate and visiting distribution into perspective.

5.3 Relaxation events and prior distributions

After having discussed the driving process, we will resolve to the relaxation dynamics. Given a certain state i, what are the chances to reach a lower state j in one jump. Generally one can decompose this transition probability into a relative transition probability $p(j \mid i)$ and a prior distribution $q(j)$. A good candidate for the prior distribution is the multiplicity of states, discussed in section 3. However as it is difficult to disentangle both distributions we will see if we can understand their combined outcome using some simple modelling assumptions.
In section 4, we mentioned that transition probabilities, which obey the scaling relation in Eq. 4.15, are good candidates for dynamics that give rise to a power law. We see in figure 40 exemplarily for 4 different measures that this assumption is already true on average. Namely, it is observed that for downward transitions of size Δi in a SSR state variable i

$$\langle \Delta i \rangle \propto i \tag{5.7}$$

holds.

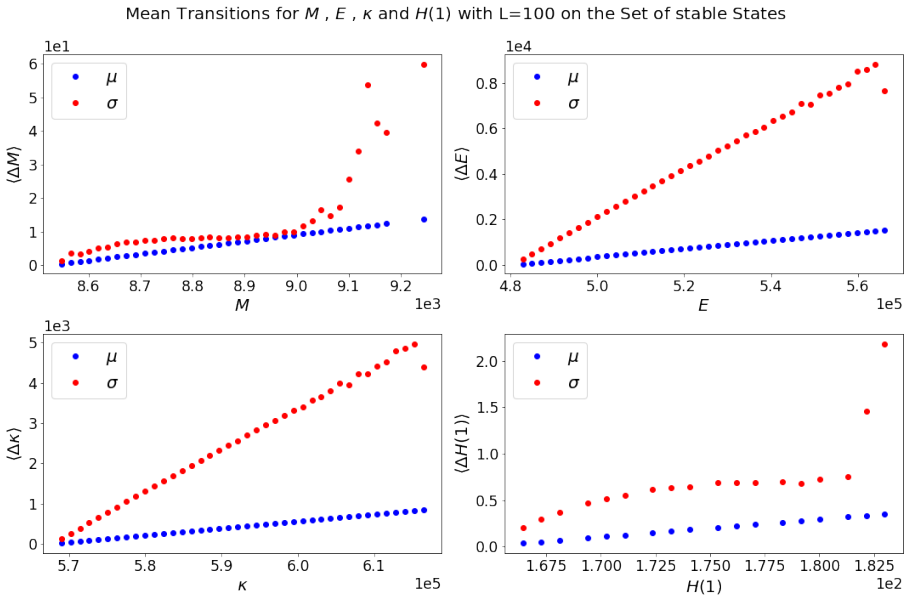

Figure 40: Shown are mean and standard deviation for the relaxation sizes of various measures. While the mean is linearly dependent on the height of the relaxing state i, the standard deviation has a less trivial dependence on i. σ of E and κ is linearly dependent, while σ of $H(1)$ and M are only in restricted regions.

If this were our only observation, we may be inclined to assume an exponential distribution for $p(j \mid i)$, as in Eq. (4.16), for a maximum entropy estimate in an analogy to the canonical ensemble. Especially for load and energy, however, the standard deviation of transition sizes from i to j is quite different than the mean, that is proportional to i, suggesting a considerable deviation from the exponential distribution. We will see that the actual dynamics are in fact more complicated.

In order to investigate this further, we study the transition probabilities visually.

- by plotting its matrix directly (see figure 41).
- by performing a data-collapse of transition probabilities on the interval $[0, 1]$. This is achieved by plotting $p(\frac{i-j}{i})$ (see figure 42).
- by representing the transition probabilities in the original interval (eg. $[E_{min}, E_{max}]$) right away (see figure 43).

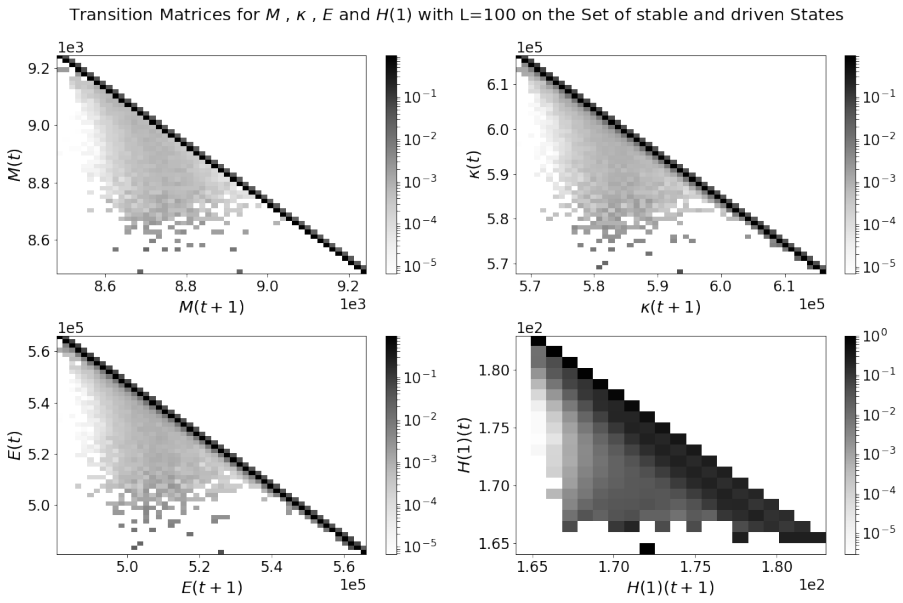

Figure 41: Shown are transition matrices for various measures. All matrices show a pronounced triangular shape. One can also see the driving process, which resides right above the diagonal. Note that states are binned in this plot.

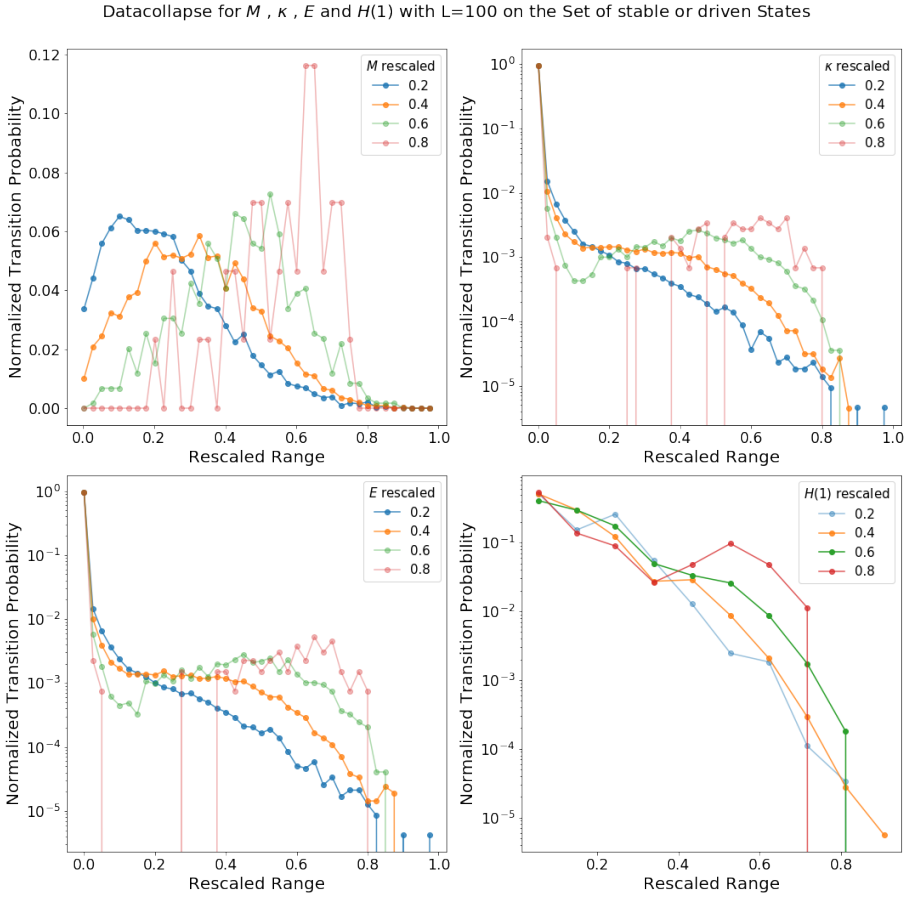

Figure 42: Normalized transition probabilities on the rescaled range $[0, 1]$. Mathematically the horizontal axis shows the relative quantity (here exemplarily for the mass): $\Delta M/(M - M_{min})$, where M is the mass at which a relaxation of size ΔM is initiated. Only non zero relaxations with $\Delta > 0$ are considered in this plot. The vertical axis gives the probability of this quantity for various initial masses (colours), which are indicated in the legend as $M/(M_{max} - M_{min})$. Further the opacity of a set of points, which correspond to an initial mass M, indicates the visiting probability of that mass. In case of the mass for instance the most frequent transitions therefore are seen as the blue and orange line.

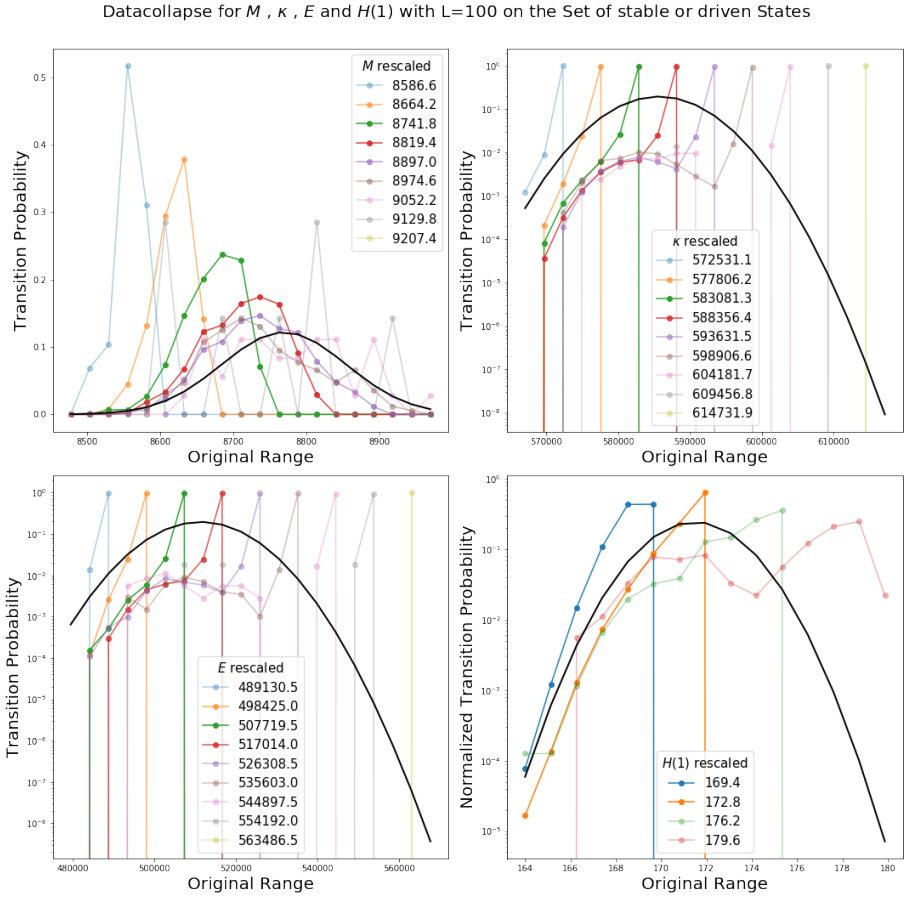

Figure 43: Transition probabilities on the original range e.g. $[\kappa_{min}, \kappa_{max}]$. Only non zero relaxations with $\Delta > 0$ are considered in this plot. The vertical axis gives the probability $p(i \mid j)$ of this quantity for various initial states i (colours). The opacity of a set of points, which correspond to an initial state i, indicates the visiting probability of that transition. The black thick lines are Gaussian probability distributions with the mean and variance chosen from the visiting distribution of the corresponding quantity.

We can distinguish 3 emerging classes of relaxations.

- Height and surface length: The size of transitions is limited in these measures to a relatively small phase space. The transition probability is more or less exponentially decaying for larger changes. A second mode is emerging for larger initial heights.

- Mass: Most of the time, mass remains constant in the system. However rarely larger avalanches occur. The transition probability takes a single moded shape. The lines do not collapse on the interval $[0, 1]$. They collapse however onto a Gaussian shape for larger initial masses on the unscaled range,

$$p(j \mid i) \propto e^{-(\mu-j)^2/2\sigma^2} \quad , \quad \text{where} \;\; j < i \quad .$$

- Energy and load: Most transitions are small, but sometimes larger avalanches occur. The single moded shape already seen for the mass, reoccurs in the tail of these transition probabilities. It is especially pronounced for higher states of energy and load. Transition probabilities corresponding to different initial energies, collapse for small avalanches onto each other in the interval $[0, 1]$. On the other hand, large avalanches condense onto a Gaussian shape in space of unscaled energies. The use of a power law multiplied by a Gaussian as transition probability is suggested as approximation,

$$p(j \mid i) \propto \frac{1}{(i-j+g)^\gamma} e^{-(\mu-j)^2/2\sigma^2} \quad , \quad \text{where} \;\; j < i \quad .$$

  γ is around -1.5. g is a free parameter that can be tuned such that the distribution fits best.
  The observation of lines lying on top of each other in the unscaled range of variables (see figure 43), hints towards the underlying prior distribution of Gaussian nature. We may choose the Gaussian to have mean and variance of the corresponding visiting distribution. This choice is made (1) due to its simplicity, (2) inspired by the shape of multiplicities $M(i)$ found in figure 3.17 and finally (3) as the assumption fits the transition probabilities reasonably well.

The emergence of the power law

Looking at the found form for the transition probabilities,

$$p(j \mid i) \propto \frac{1}{(i-j+g)^{\gamma}} e^{-(\mu-j)^2/2\sigma^2} \quad ,$$

it still remains unclear how the power law $(i-j+g)^{\gamma}$ comes about. As of now we only observe that the power law with roughly an exponent of -1.5, which is featured in the avalanche distribution, is already present in the constituting transition probabilities. Christensen and Moloney [19] present the derivation of the avalanche size probability in a special form of the BTW model, namely the BTW model with random neighbours. The result is a scaling form of the avalanche size probability. I will present a sketch of the proof here and argue by analogical reasoning that a similar situation can be found for the Oslo model. For details please refer to [19] or this review by Corral and Font-Clos [36].
In the 2D BTW model with random neighbours, if a site x_i reaches the fixed threshold z, its grains are distributed to z randomly chosen neighbours x_1, x_2, $\ldots$, x_z, which subsequently may be toppling themselves. The probability to induce a further toppling event will be called p. This situation can be seen as a branching process, where at each node a maximum of z branches are induced with probability p. Any branch terminates in another node. Over the course of a longer avalanche a tree is spanned by these branches. We will be interested in the case of $z = 2$. Then the probability to find an avalanche of size $s \geq 1$ can be derived.

$$P(s,p) = \frac{1}{s+1}\binom{2s}{s}\frac{1-p}{p}\left(p(1-p)\right)^s \tag{5.8}$$

Here $M(s) = \frac{1}{s+1}\binom{2s}{s}$ is the multiplicity of such trees, which was already derived in [37], while the remainder gives the probability. Using Stirling formula $M(s)$ can be approximated for large s,

$$M(s) \approx \frac{1}{\sqrt{\pi}} s^{-3/2} 4^s \quad .$$

In case $p = 1/2$ the avalanche size probability becomes a pure power law for large s,

$$P(s,p) \approx s^{-3/2} \quad . \tag{5.9}$$

If p is sufficiently close to $1/2$ a power law with exponential cut-off is found.
In case of the Oslo model, the situation is different in three ways. Firstly, the system is 1D, not 2D, secondly, the neighbours are not chosen randomly and thirdly, the probability to induce topplings in neighbours downstream is larger than inducing them upstream. Nevertheless the general form for the multiplicities remains the same. This may inspire us to argue that the power law results from a cascade of avalanches.

5.4 The Oslo model as a SSR process

Now let us put together these findings. After we have gathered analytical models and estimates for the driving and relaxation process it is now possible to compare these results. We will present the results for the load as dynamical variable.
As a first step the large number of observed load states are course grained into N equidistant discrete bins of size b,

$$b = \frac{\kappa_{max} - \kappa_{min}}{N} \quad .$$

Here κ_{max} and κ_{min} are the largest and smallest loads observed in simulation. To arrive with the expected visiting distribution of loads we assumed a transition matrix of the form

$$p(j \mid i) = \begin{cases} \frac{1}{2Z_i} \frac{1}{(i-j+g)^{1.55}} e^{-(\mu-j)^2/2\sigma^2} & i > j \\ 1/2 & j = i + k \end{cases} \quad . \tag{5.10}$$

Here μ and σ are the mean and standard deviation of the observed visiting distribution. $g > 0$ is a free parameter. In this case the parameters Z_i and k are defined in the following way

$$k = \left\lfloor \frac{L}{N} \right\rfloor + 1 \quad , \tag{5.11}$$

$$Z_i = \sum_{j=1}^{i} \frac{1}{(i-j+g)^{1.55}} e^{-(\mu-j)^2/2\sigma^2} \quad . \tag{5.12}$$

L is the gain in κ at each driving event. It is divided by the number of bins N in order to arrive with the gain in κ on the rescaled range. It is rounded up in order to make sure that large bin sizes can not lead to $k = 0$, because this would result in an attractor configuration saturated in the bin of lowest load κ_{min} only.
In figure 44 the final result is shown for the avalanche distribution. The analytic curve (blue) can reproduce the general form of the observed avalanche distribution (red). We can now conclude that a complex enough SSR picture can reproduce the statistics of the Oslo model. With the current model, this is however only possible to a certain level of accuracy. In the next section I would like to point to some problems with the model and how they could be resolved.

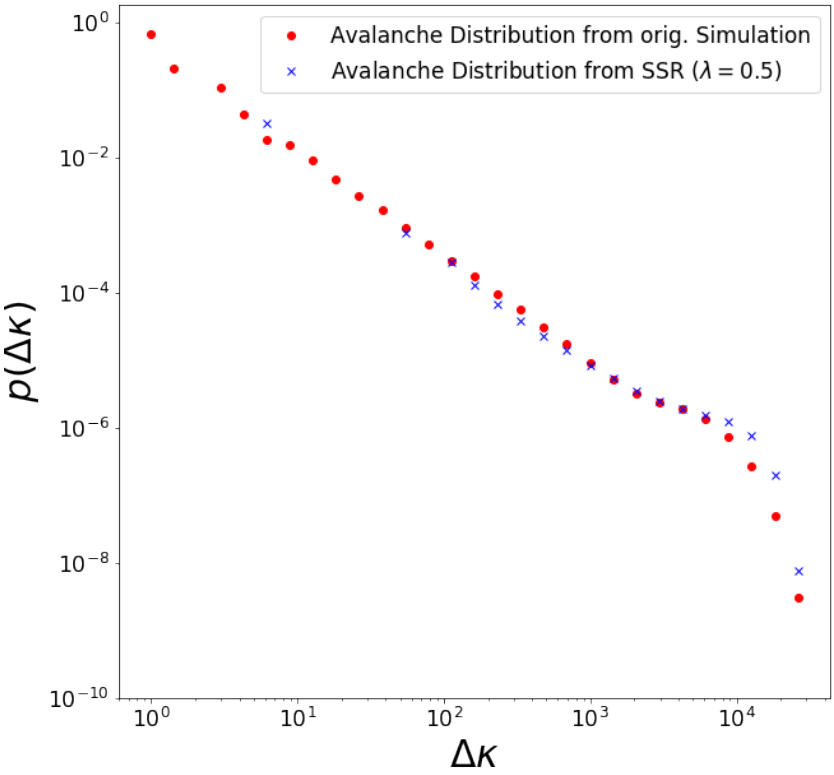

Figure 44: Red points: Avalanche Distribution as measured in a simulation of the Oslo model with $p = 0.5$ and $L = 100$. Blue points: Analytically derived avalanche size distribution. A binned space with $N = 500$ bins is created, on which a transition matrix, Eq. (5.10), acts. Here μ and σ are taken from the measured visiting distribution. $g = 0.1$ was chosen as a fitting parameter. k was measured according to Eq. (5.11). $\lambda = 0.5$ was used as previous investigation into the driving rate suggest. An analytic visiting distribution is derived as the eigenvector corresponding to the largest eigenvalue of the transition probability. From this analytic visiting distribution the avalanche distribution can be derived using Eq. (4.17). For details on the plotting method used, see the appendix in chapter A below.

5.5 Discussion and outlook

The final result is given by the avalanche distribution in figure 44. We can also compare the resulting visiting distributions (see figure 45). While the observed distribution and the calculated visiting distribution obey a similar shape, their relative position is different. By the end of my project, I was not able to clearly identify the reason for that offset. It could be that the parameter g in the final model induces this deviation.

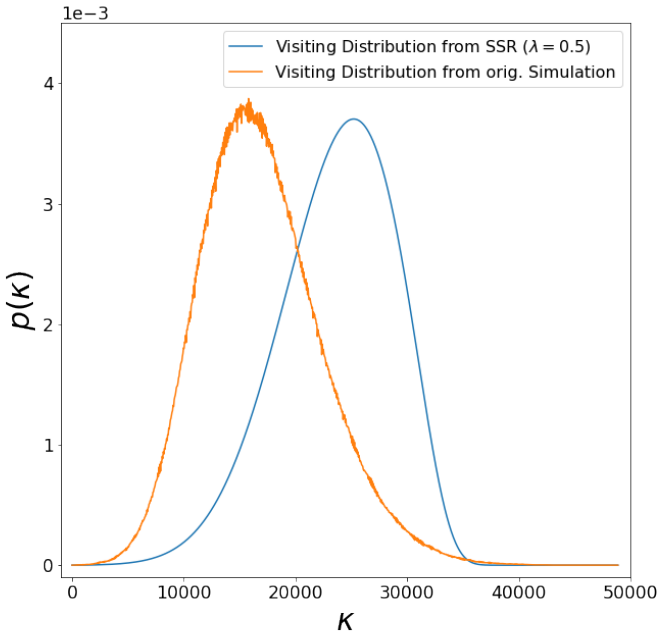

Figure 45: The visiting distribution of the load κ for the same parameters as in figure 44. The orange line is the observed visiting distribution in the Oslo model, while the blue line gives the load distribution derived with the described SSR model. The two distributions show a similar qualitative shape. The maximum of the computed distribution is however shifted to the higher values of κ compared to the observed distribution.

At the end of this thesis I have arrived with a simplified model that can roughly reproduce the dynamics of the Oslo sandpile. Note however that, despite the success of applying SSR mechanisms to this problem, the actual nature of the power law in the avalanche distributions was not explained. We successfully identified the exponential cut-off as a result of an underlying prior distribution.

The transition probability was however forced to be a power law and did not result from a microscopic description. A possible bottom-up explanation could be achieved via understanding the dynamics of an avalanche as a branching process and we showed that this line of thinking may be fruitful by comparing the dynamics with the BTW model with random neighbours as presented in [19]. The literature on SSR processes provides two explanations for power laws of exponent smaller than -1. First, the prior distribution could have an exponent < -1 [26] or secondly, the underlying dynamics are describable by a cascading event [27]. It will be interesting for future research to investigate the relationship between cascading and branching processes. The avalanches of the Oslo model provide a system which could potentially be described as both.

We have made the observation that the visiting distributions of macrostates in the Oslo model show roughly Gaussian shapes (see figure 33), with a slightly higher kurtosis. Further, their position and variance appear to be a good estimate for the Gaussian prior distributions. The SSR relaxation transition probabilities contain an absolute Gaussian term that was modelled using mean and variance of the visiting distributions. This suggests that the visiting distribution collapses in fact onto the prior distributions. Otherwise it would not be so evidently visible in the transition probabilities (figure 43). The form of the prior distribution could be associated with the multiplicity of states in the system (figure 3.17). This will in general depend of the value of the toppling probability p. p can be believed to shift the center of the Gaussian prior distribution to the left or right. By the end of this work we still lack an analytical result for the dependence of the multiplicity on the value of p. I encourage later research to investigate this matter further.

6 Conclusion

In my work I was investigating some SSR characteristics of the Oslo sandpile model, thereby indicating that the SSR framework is applicable to driven non-equilibrium systems such as sandpiles, as a descriptive tool.

This was shown in particular for the case of the Oslo sandpile model. The OSM is subject to simple rules that lead to non-Gaussian statistics. The distribution of avalanche sizes is following a power law distribution with power -1.55. We have defined a set of macro variables that allows us to study the Oslo model in the mathematical framework of SSR processes. Avalanches can then be associated to movements in a phase space spanned by those macro variables and we observed the existence of "stochastic limit cycles" within it, illustrating that the Oslo model is a non-equilibrium system balanced by driving and relaxation. Utilizing the existing theory of SSR processes and extending it, we were able to remodel the driving and relaxation events of the Oslo sandpile. We calculated and measured the rate of driving, the type of driving and the relaxation transition probability by performing simulations. A prior distribution was observed in the statistics of the relaxation transition probability and was associated with the multiplicity of macrostates in the Oslo model. Finally, the form of the avalanche size distribution was successfully remodelled using SSR processes. The maximum of the modelled visiting distribution, however, does not fit the observed distribution in the present model. To that end the model still requires improvement.

We found a simplified and analytical SSR model for the dynamics of state and avalanche probabilities in the OSM. This model however is as such descriptive. It does not *explain* the origin of scale-free avalanche sizes in sandpiles. While the Gaussian cut-off, observed as part of the avalanche distribution, could origin from the multiplicities of energy states in the OSM, the power law itself was assumed as a modelling input. Simple non-cascading SSR processes can produce power laws of power α in their visiting distribution, where $\alpha \in (0, -1]$, and can therefore not predict the observed power law of the avalanche distribution. This does however not exclude the possibility that the power law could in principle be explained by SSR dynamics in a non-trivial way. It is to argue that a branching process, expressed by the cascading character of the avalanches, could by itself be modelled as a SSRP. Further research on this topic will therefore focus on the cascading character of avalanches in the Oslo model.

A Data Representation

We are given some observations of N events X_i in an interval $[x_{min}, x_{max}]$. As the available data is limited, we choose to define bins i with length $b_i = x_{u,i} - x_{l,i}$ and data points falling onto them $n(b_i)$. Theoretically for $N \to \infty$ and $b_i \to 0$ we expect:

$$\frac{n(i)}{b_i N} \to p(x)$$

For sufficient amounts of data, we therefore assume:

$$\frac{n(i)}{b_i N} \approx p(x) \tag{A.1}$$

In this thesis, bins of constant size ($b_i = \text{const.}$) and exponentially growing bins ($b_i \propto a^i$) were used. In order to indicate data points corresponding to different bins i in a graph we will either choose the lower bin edge $x_{l,i} = x_i$ on a linear axis, or the geometric mean of both bin edges $x_i = \sqrt{x_{u,i} \cdot x_{l,i}}$ on a logarithmic axis.
In figure 44 the avalanche sizes, measured throughout a simulation of the Oslo model are clustered in exponentially growing bins (red points). In this way, the noise in the tail of the avalanche distribution is visually reduced. In the same plot we also present data points generated by a corresponding SSR process (blue crosses). The avalanche distribution given by the SSR method is a histogram with bins of constant size. For means of comparison this histogram on constant bin sizes is transformed into a histogram that lives on the same exponentially growing bins, as the red points (simulation data) do. In order to achieve this, we ask how many N_i constant bin positions x_j fall into a larger exponentially growing bin with index i. For all those constant bins at positions x_j the average frequency $\tilde{f}_i = \sum f_j / N_i$ (height of a rectangle in the histogram) is computed. Those average frequencies are presented as blue crosses.

B Abstract

Critical phenomena within equilibrium thermodynamics are quite well understood and their theory makes precise predictions on scaling behaviours near the critical point. Self-organized criticality, a term coined by Per Bak, was introduced as an extension of this concept to explain the emergence of power laws in driven systems. The Oslo sandpile model (Oslo model), a model for a 1+1 dimensional sandpile, for instance shows power law distributions in the frequency of avalanche sizes and was extensively studied. While there has been some success, the approach still lacks generality and the power to produce exact results. Recently another route to out-of-equilibrium systems, namely the Driven Sample Space Reducing Process (SSR), was proposed. The aim of my thesis is to show that SSR processes are at the heart of sandpile dynamics as demonstrated with the Oslo model.

C Zusammenfassung

Die Theorie der Thermodynamik macht genaue Vorhersagen über das Verhalten von Systemen nahe eines kritischen Punkts, solange sich diese Systeme im thermodynamischen Gleichgewicht befinden. Das Prinzip der Selbstorganisierten Kritikalität wurde von Per Bak zur Erklärung kritischen Verhaltes und des Auftretens von endlastigen Verteilungen in getriebenen Systemen vorgeschlagen. Als Beispiel kann das viel studierte Oslo Sandhaufen Modell (Oslo Modell) angeführt werden, welches das dynamische Verhalten eines 1+1 dimensionalen getriebenen Sandhaufens beschreibt. Die statistische Verteilung der Lawinengrößen, welche sich von dem Sandhaufen im Oslo Modell lösen, folgt einem Potenzgesetz. Die Anwendung des Prinzips der selbstorganisierten Kritikalität auf das Oslo Modell war bisher nur teilweise erfolgreich. In dieser Masterarbeit wähle ich eine neue Herangehensweise an das kritische Verhalten von Sandhaufen. Ich beschreibe ihre Dynamik und im Speziellen das Oslo Modell mithilfe eines Phasenraum Reduzierenden Prozesses und zeige, dass solche Prozesse die grundsätzliche Natur von Lawinen auf getriebenen Sandhaufen wiedergeben können.

References

[1] Ilya Prigogine. Time, structure and fluctuations. *Nobel Lectures in Chemistry 1971-1980*, pages 263–285, 1977.

[2] Lars Onsager. Reciprocal relations in irreversible processes. i. *Physical review*, 37(4):405, 1931.

[3] Edwin T Jaynes. The minimum entropy production principle. *Annual Review of Physical Chemistry*, 31(1):579–601, 1980.

[4] Leonid M Martyushev and Vladimir D Seleznev. Maximum entropy production principle in physics, chemistry and biology. *Physics reports*, 426(1):1–45, 2006.

[5] Edwin T Jaynes. *Probability theory: The logic of science*. Cambridge university press, 2003.

[6] Purushottam D Dixit, Jason Wagoner, Corey Weistuch, Steve Pressé, Kingshuk Ghosh, and Ken A Dill. Perspective: Maximum caliber is a general variational principle for dynamical systems. *The Journal of chemical physics*, 148(1):010901, 2018.

[7] Michael J Hazoglou, Valentin Walther, Purushottam D Dixit, and Ken A Dill. Communication: Maximum caliber is a general variational principle for nonequilibrium statistical mechanics, 2015.

[8] Per Bak, Chao Tang, and Kurt Wiesenfeld. Self-organized criticality: An explanation of the 1/f noise. *Physical review letters*, 59(4):381, 1987.

[9] Vidar Frette, Kim Christensen, Anders Malthe-Sørenssen, Jens Feder, Torstein Jøssang, and Paul Meakin. Avalanche dynamics in a pile of rice. *Nature*, 379(6560):49, 1996.

[10] Kim Christensen, Hans C Fogedby, and Henrik Jeldtoft Jensen. Dynamical and spatial aspects of sandpile cellular automata. *Journal of statistical physics*, 63(3-4):653–684, 1991.

[11] William H Press. Flicker noises in astronomy and elsewhere. *Comments on Astrophysics*, 7:103–119, 1978.

[12] Albert-László Barabási and Réka Albert. Emergence of scaling in random networks. *science*, 286(5439):509–512, 1999.

[13] Benoit Mandelbrot. An informational theory of the statistical structure of language. *Communication theory*, 84:486–502, 1953.

[14] Nigel Goldenfeld. *Lectures on phase transitions and the renormalization group*. CRC Press, 2018.

[15] Ernst Ising. Contribution to the theory of ferromagnetism. *Z. Phys.*, 31:253–258, 1925.

[16] Markus J Aschwanden, Norma B Crosby, Michaila Dimitropoulou, Manolis K Georgoulis, Stefan Hergarten, James McAteer, Alexander V Milovanov, Shin Mineshige, Laura Morales, Naoto Nishizuka, et al. 25 years of self-organized criticality: Solar and astrophysics. *Space Science Reviews*, 198(1-4):47–166, 2016.

[17] Nicholas W Watkins, Gunnar Pruessner, Sandra C Chapman, Norma B Crosby, and Henrik J Jensen. 25 years of self-organized criticality: Concepts and controversies. *Space Science Reviews*, 198(1-4):3–44, 2016.

[18] Per Bak and Kan Chen. The physics of fractals. *Physica D: Nonlinear Phenomena*, 38(1-3):5–12, 1989.

[19] Kim Christensen and Nicholas R Moloney. *Complexity and criticality*, volume 1. World Scientific Publishing Company, 2005.

[20] Alvaro Corral. Calculation of the transition matrix and of the occupation probabilities for the states of the oslo sandpile model. *Physical Review E*, 69(2):026107, 2004.

[21] Deepak Dhar. Theoretical studies of self-organized criticality. *Physica A: Statistical Mechanics and its Applications*, 369(1):29–70, 2006.

[22] Gunnar Pruessner. Oslo rice pile model is a quenched edwards-wilkinson equation. *Physical Review E*, 67(3):030301, 2003.

[23] Joseph G Eisenhauer. Regression through the origin. *Teaching statistics*, 25(3):76–80, 2003.

[24] Alvin Chua and Kim Christensen. Exact enumeration of the critical states in the oslo model. *arXiv preprint cond-mat/0203260*, 2002.

[25] Bernat Corominas-Murtra, Rudolf Hanel, and Stefan Thurner. Understanding scaling through history-dependent processes with collapsing sample space. *Proceedings of the National Academy of Sciences*, 112(17):5348–5353, 2015.

[26] Bernat Corominas-Murtra, Rudolf Hanel, and Stefan Thurner. Extreme robustness of scaling in sample space reducing processes explains zipfs law in diffusion on directed networks. *New Journal of Physics*, 18(9):093010, 2016.

[27] Bernat Corominas-Murtra, Rudolf Hanel, and Stefan Thurner. Sample space reducing cascading processes produce the full spectrum of scaling exponents. *Scientific reports*, 7(1):11223, 2017.

[28] Stefan Thurner, Rudolf Hanel, Bo Liu, and Bernat Corominas-Murtra. Understanding zipf's law of word frequencies through sample-space collapse in sentence formation. *Journal of the Royal Society Interface*, 12(108):20150330, 2015.

[29] Avinash Chand Yadav. Correspondence between a noisy sample-space-reducing process and records in correlated random events. *Physical Review E*, 96(3):032134, 2017.

[30] Bernat Corominas-Murtra, Rudolf Hanel, Leonardo Zavojanni, and Stefan Thurner. How driving rates determine the statistics of driven non-equilibrium systems with stationary distributions. *Scientific reports*, 8(1):10837, 2018.

[31] Rudolf Hanel and Stefan Thurner. Maximum configuration principle for driven systems with arbitrary driving. *Entropy*, 20(11):838, 2018.

[32] Rudolf Hanel, Stefan Thurner, and Murray Gell-Mann. How multiplicity determines entropy and the derivation of the maximum entropy principle for complex systems. *Proceedings of the National Academy of Sciences*, 111(19):6905–6910, 2014.

[33] Paczuski Maya and Boettcher Stefan. Transport in sand piles, interface depinning, and earthquake models. *Phys. Rev. Lett*, 77:111–114, 1996.

[34] Seng Cheang and Gunnar Pruessner. The edwards–wilkinson equation with drift and neumann boundary conditions. *Journal of Physics A: Mathematical and Theoretical*, 44(6):065003, 2011.

[35] Stephen Kokoska and Daniel Zwillinger. *CRC standard probability and statistics tables and formulae*. Crc Press, 2000.

[36] Alvaro Corral and Francesc Font-Clos. Criticality and self-organization in branching processes: application to natural hazards. *arXiv preprint arXiv:1207.2589*, 2012.

[37] Geoffrey Grimmett. What is percolation? In *Percolation*, pages 1–31. Springer, 1999.